Manuscript prepared for Atmos. Chem. Phys. Discuss.
with version 2.2 of the LaTeX class copernicus_discussions.cls.
Date: 20 June 2014

Transport of aerosol to the Arctic: analysis of CALIOP and French aircraft data during the spring 2008 POLARCAT campaign

G. Ancellet[1], J. Pelon[1], Y. Blanchard[1], B. Quennehen[2,1], A. Bazureau[1], K.S. Law[1], and A. Schwarzenboeck[2]

[1]Sorbonne Université, UPMC, Paris 06; Université Versailles St-Quentin; CNRS/INSU; LATMOS
[2]Université B. Pascal; INSU/CNRS; Laboratoire de Météorologie Physique

Correspondence to: G. Ancellet (gerard.ancellet@upmc.fr)

Abstract

Lidar and in situ observations performed during POLARCAT campaign are reported here in terms of statistics to characterize aerosol properties over northern Europe using daily airborne measurements conducted between Svalbard Island and Scandinavia from 30 March to 11 April 2008. It is shown that during this period, a rather large number of aerosol layers was observed in the troposphere, with a backscatter ratio at 532 nm of 1.2 (1.5 below 2 km, 1.2 between 5 and 7 km and a minimum in-between). Their sources were identified using multispectral backscatter and depolarization airborne lidar measurements after careful calibration analysis. Transport analysis and comparisons between in situ and airborne lidar observations are also provided to assess the quality of this identification. Comparison with level 1 backscatter observations of the spaceborne CALIOP lidar were carried out to adjust CALIOP multispectral observations to airborne observations on a statistical basis. Re-calibration for CALIOP daytime 1064 nm signals leads to a decrease of their values by about 30% possibly related to the use of the Version 3.0 calibration procedure. No re-calibration is made at 532 nm even though 532 nm scattering ratios appear to be biased low (-8%) because there are also significant differences in air mass sampling between airborne and CALIOP observations. Re-calibration of the 1064 nm signal or correction of -5% negative bias in the 532 nm signal both could improve the CALIOP aerosol color ratio expected for this campaign. The first hypothesis was retained in this work. Regional analyses in the European Arctic performed as a test, emphasize the potential of the CALIOP spaceborne lidar to further monitor ~~more~~ in depth properties of the aerosol layers over the Arctic using infrared and depolarization observations. The CALIOP April 2008 global distribution of the aerosol backscatter reveal two regions with large backscatter below 2 km: the Northern Atlantic between Greenland and Norway, and Northern Siberia. The aerosol color ratio increases between the source~~s~~ regions and the observations at latitudes above 70°N is consistent with a growth of the aerosol ~~size~~ once transported to the Arctic. The distribution of the aerosol optical properties in the mid troposphere supports the known main transport pathways between mid-latitudes and the Arctic.

1 Introduction

It is recognized that long range transport of anthropogenic and biomass burning emissions from lower latitudes is the primary source of aerosol in the Arctic (Quinn et al., 2008; Warneke et al., 2010). Frequent haze and cloud layers in the winter-spring period contribute to surface heating by their infrared emission (Garrett and Zhao, 2006). The relative influence of the different mid-latitude aerosol sources was initially discussed by Rahn (1981) who concluded that the Eurasian transport pathway is important using meteorological considerations and observations. Law and Stohl (2007) also stressed the seasonal change of air pollution transport into the Arctic with a faster winter circulation implying a stronger influence of the southerly sources in the middle and upper troposphere.

During the International Polar Year in 2008, these questions were addressed in the frame of the Polar Study using Aircraft, Remote Sensing, Surface Measurements and Models, Climate, Chemistry, Aerosols and Transport (POLARCAT) and Arctic Research of the Composition of the Troposphere from Aircraft and Satellites (ARCTAS) field experiments. Aircraft observations were conducted respectively in spring 2008 over the European Arctic as part of POLARCAT-France (Adam de Villiers et al., 2010; Quennehen et al., 2012) and over the North American Arctic as part of ARCTAS (Jacob et al., 2010). Several papers have already been published on the characterization of aerosols over the western Arctic (Brock et al., 2011; Rogers et al., 2011; Shinozuka et al., 2011). Overall they provide a very useful data base to discuss the aerosol transport pathways and the main processes driving their evolution when transported to the Arctic. Besides field experiments involving aircraft measurements, no systematic information was provided until recently on regional Arctic aerosols by space observations. The Cloud-Aerosol Lidar and Infrared Pathfinder Satellite Observation (CALIPSO) mission (Winker et al., 2009) has proven to be very useful to address these questions as illustrated by the recent work of Winker et al. (2013) although all its potential has not been explored yet. Recent studies using the Cloud-Aerosol Lidar with Orthogonal Polarization (CALIOP) level 2 products, namely the 5 km aerosol layer products (AL2) at 532 nm gridded for the Arctic domain allowed aerosol extinction and aerosol optical depth (AOD) to be derived (Di Pierro et al., 2013). The main

features of transport in the Arctic were inferred from the seasonal variability of the vertical distribution of aerosol, derived from AL2 version 3 products by Devasthale et al. (2011). Observations by the CALIOP lidar provide the optical properties of aerosol layers at two different wavelengths (532 nm, 1064 nm), but the infrared (IR) data have not been widely used due in a large part to difficulties in the calibration of the level 1 (L1) products (Wu et al., 2011; Vaughan et al., 2012)). In our study we thus address this topic looking for the usefulness of the additional information provided by the 1064 nm channel and depolarization measurements.

In this work, we focus on the European Arctic sector in spring 2008 using the data of the POLARCAT-France experiment. The purpose of this paper is thus to discuss how CALIOP spaceborne lidar data can be compared to and combined with aircraft data in the western Arctic area to provide (i) a comparison of CALIOP observations with those from airborne lidar at similar wavelengths in a region where CALIOP data are very useful but not very well characterized (ii) tracks for bias correction and use of L1 CALIOP observations at 1064 nm and in the depolarization channel to analyze behavior of color and depolarization ratios, respectively. (iii) an improved description of the spatial variability of aerosol sources and transport to the Arctic, and implications for a regional and monthly mean characterization.

We start in section 2 by a description of the aircraft campaign lidar data and the meteorological context which includes also a characterization of the particles from in situ measurements and air mass transport using the FLEXPART model. The POLARCAT France campaign was only described for some specific flights in previous papers (Adam de Villiers et al., 2010; Quennehen et al., 2012). In section 3.3, comparison between airborne and spaceborne data are addressed, looking to the statistical distribution and the spatial variability derived from all the aircraft flights available during POLARCAT-France, and coordinated CALIOP observations. In section 4, results obtained with monthly averaged L1 CALIOP data in April 2008 are used to analyze (i) the link between the meridional variability of the aerosol properties in relation with the air mass origin (ii) the large scale horizontal variability in these aerosol properties in the whole Arctic domain. The latter is finally discussed with respect to the results obtained by previous analysis involving CALIOP AL2 products.

2 The POLARCAT spring campaign

2.1 Campaign context and description

The French ATR-42 was equipped with remote sensing instruments (lidar, radar), in-situ measuring probes of gases (O3, CO) and aerosols (concentration, size distribution). The ATR-42 deployment was often designed to collect data near to CALIOP satellite observations during daytime overpasses. The positions of the 12 scientific flights performed from 30 March to 11 April 2008 (Fig.1) show that they are well suited for an analysis of the meridional distribution near 20°E. The meteorological context in the Arctic in April 2008 is discussed in Fuelberg et al. (2010). The maps of the 700 hPa equivalent potential temperature (θ_e) and winds are however shown in figure 1 and 2 of the supplementary information document to identify the variability of the position of the Arctic front. This front was near 71°N until 2 April and moved to lower latitudes near 68°N after 2 April. It is seen that flights were frequently performed in the air masses strongly influenced by the southerly flow from Europe at the beginning of the campaign, while large section of the flights were representative of the Arctic pristine air at the end of the campaign. After 9 April, the European Arctic at latitude above 70°N becomes strongly influenced by advection of biomass burning plumes advected from Asia (Quennehen et al., 2012).

The vertical structure of the aircraft flight plans were always chosen to have several in-situ and airborne lidar measurements in similar air masses in order to study the representativeness of lidar products such as the attenuated backscatter, the color ratio and the depolarization ratio.

During the aircraft campaign, the CALIOP spaceborne instrument provided 80 satellite overpasses for the period 27 March to 11 April in the area: 65°N-80°N, 5°E-35°E (Fig.1). For the area south of 72.5°N which corresponds to the aircraft deployment, there are 45 CALIOP tracks leading to 433 vertical profiles with 80 km horizontal resolution. In this work different temporal or spatial averaging will be used to analyze the CALIOP data either in the aircraft domain for comparison with the airborne data (section 3.3) or in the whole European Arctic area for all the days in April 2008 (section 4).

2.2 Aircraft data

2.2.1 Airborne Lidar measurements

During the POLARCAT campaign, the airborne lidar LEANDRE Nouvelle Generation, provided measurements in its backscatter configuration (hereafter simplified as B-LNG) of total attenuated backscatter vertical profiles at three wavelengths: 355, 532 and 1064 nm. An additional channel recorded the perpendicular attenuated backscatter vertical profile at 355 nm. The B-LNG lidar is already described in Adam de Villiers et al. (2010) (ADV2010) where a single flight on 11 April 2008 was analyzed. The methodology to calibrate the attenuated backscatter is also fully described in ADV2010 so it is only briefly described here.

In this paper, aerosol layers are identified for the 12 flights using 20-s averages of lidar profiles (i.e. a 1.5 to 2 km horizontal resolution). Only downward pointing lidar observations have been included in this work. The B-LNG data are first corrected for energy variations. Calibration factors are then determined for each wavelength and for each flight by searching for areas with very low aerosol content and by assuming that the Rayleigh contribution controls the lidar signal. These areas are chosen, as far as possible, in the upper altitude range close to the aircraft where bias due to the aerosol transmission does not play a significant role. The consistency of the calibration factor is checked using different aerosol free areas, and several flights, whenever possible. This is the major source of error in the calculation of $R(z)$, and the uncertainty (error + bias, but mostly due to bias) was found to be less than 15% at 532 nm and less than 30% at 1064 nm. These numbers were derived from a sensitivity study using different possible calibration factors and different flights. The two 355 nm channels are calibrated independently using molecular reference and the ratio of the total perpendicular- to the total parallel-polarized signals. However, due to a reduced field of view at 355nm, the overlap of the emitted beam with the receiver field of view limits our ability to calibrate independently the total 355 nm lidar signal in the areas near the aircraft selected at the other wavelengths. Therefore, and as CALIOP is operating at 532 nm, the measurements at 355 nm are only used for the depolarization ratio analysis, which is less dependent on the geometrical factor. The B-LNG 355 nm ratio is only a proxy for the CALIOP one, as some differences are expected to occur due to wavelength

difference (Freudenthaler et al., 2009).

The aerosol parameters discussed in this paper and the way to calculate them, are fully described in ADV2010. They are the same for airborne and spaceborne observations (although depending on the wavelength for depolarization). They are namely (i) the attenuated backscatter ratios $R(z)$ at 532 nm and 1064 nm using the CALIOP atmospheric density model to calculate the Rayleigh backscatter vertical profiles, (ii) the ratio of the total perpendicular- to the total parallel plus perpendicular polarized backscatter coefficient (or pseudo depolarization ratio (PDR) δ_{355}) at the measurement wavelength, 355 or 532 nm, respectively, (iii) the pseudo color ratio defined as the ratio of the total backscatter coefficients at 1064 and 532 nm ($PCR(z)$=$R_{1064}(z)$/[$16R_{532}(z)$] (iv) the color ratio defined as the ratio of the aerosol backscatter coefficients at 1064 and 532 nm ($CR_a(z)$=($R_{1064}(z)-1$)/[$16(R_{532}(z)-1)$]). The aerosol color ratio can be also written as $CR_a(z) = 2^{-k}$, where k is an exponent depending on the aerosol microphysical properties (Cattrall et al., 2005).

The vertical and latitudinal aircraft cross sections are listed in Table 1 and the corresponding R_{532} sections are shown in Fig.3 of the supplementary information document. Clouds are removed from the lidar signals using a threshold both in scattering ratio and depolarization.

This dataset composed of 18 lidar meridional cross sections is a representative sample of the European Arctic spring aerosol distribution, as it includes different kinds of aerosol load in the lower troposphere and several cases of aerosol layers detected in the troposphere above 2 km. The probability density function (PDF) of the retrieved $R(z)$ are shown in Fig.2 to check that the lidar data processing does not produce outliers for some flights. The homogeneity of the results between the different flights has also been verified by dividing the lidar data into three subsets: one corresponding to the beginning of the campaign (before 7 April) , the second one to the end (after April 7), and the third to the overall campaign (see Table 1) . The differences between the 3 subsets are small when looking at the means and standard deviations of the distributions meaning that the error related to the calibration procedure is independent of the selected flight (not shown). In Fig.2, the $R_{532}(z)$ values do not exceed 2 (90th percentile=1.45) with a mean value of 1.2, as expected for the Arctic troposphere where there are a lot of air masses with a low aerosol load (Rodríguez et al., 2012). Both the IR and the green distribution

show a high left tail in the histogram. Although most of the aerosol scattering ratios are found near the median values (R_{532}=1.15 and R_{1064}=1.9), the high left tail shows that air masses with R_{532} >1.4 and R_{1064} >2.8 are also frequently found (probability > 75%). The uncertainty of the mean values $\overline{R_{532}}$ and $\overline{R_{1064}}$ can be evaluated assuming 100 independent samples for the 18 cross sections shown in Fig.3 of the supplementary document, (i.e. 3 vertical layers and 2 horizontal layers) and errors of 0.1 and 0.5 for R_{532} and R_{1064}, respectively, in a single layer. The distribution of the aerosol color ratio shows a mean $\overline{CR_a}$ near 0.31±0.12, corresponding to a rather large wavelength dependence, and thus to small particle size (k=2). A small mode is seen to occur near 0.5 corresponding to much smaller wavelength dependence (k=1) and thus to larger particles. We also obtain a value of 0.33± 0.04 for the color ratio $\overline{CR_a}^* = \frac{\overline{R_{1064}}-1}{16(\overline{R_{532}}-1)}$ calculated using the mean values of $R(z)$ (Fig.2). Larger values near 0.5 are explained by the fact that at least 20% of the 532 nm observations with moderate R_{532} values near 1.2 contribute to the tail of the R_{1064} distribution with values more than 2.4. The CR_a values from the B-LNG are smaller than the range 0.4-1 (dust excepted) derived from the AERONET network using sun photometers at 26 sites across the globe (Cattrall et al., 2005). However similar values have been reported for polar air masses using lidar measurements in Alaska and Canada (Burton et al., 2012) and for a smoke layer over Ny-Alesund (Stock et al., 2011).

Since in Fig. 2, the backscatter ratio distributions points toward a significant contribution of aerosol particles with small sizes, we thus looked at in situ measurements where comparisons are possible.

2.2.2 Comparison of airborne lidar with in-situ measurements

Aerosol and carbon monoxide (CO) in-situ measurements available on the ATR-42 aircraft are described in Quennehen et al. (2012) and ADV2010. For the aerosols, a condensation particle counter (CPC-3010) measured the number of submicronic particles, while the aerosol concentrations in different size bins were measured by a Passive Cavity Aerosol Spectrometer Probe (PCASP SPP-200), a GRIMM (model 1.108), and a Scanning Mobility Particle Sizer (SMPS) with a lower time resolution (150 s). In this paper we have used the SMPS and the

Grimm data to compute the aerosol mean geometrical diameter with the 150 s time resolution. Comparisons of the CPC concentrations with the integrated concentrations of the 8 size bins of the GRIMM between 0.3 and 3 μm, provide estimates of the relative fractions of coarse size aerosol.

For flights with frequent vertical motion of the aircraft, it is easy to verify the comparability of lidar and in-situ data. Such a comparison involves looking at in-situ measurements only during aircraft ascents or descents crossing aerosol layers that the lidar detects later or earlier, respectively. An example of a comparison of the lidar attenuated backscatter measured 150 m below the aircraft with CO and the CPC concentrations is shown in Fig.3 for the last flight on 11 April 2008, where rather large aerosol scattering ratios were measured (see Fig.3 of the supplementary information document). No delay correction is performed in this figure to compensate for aircraft speed and lidar measurement distance (this is not detectable at this scale), but a high correlation (0.55 with a significance better than 99%) is nevertheless observed between lidar backscatter ratio and aerosol particle concentration.

Ten independent aerosol layers seen at nearly the same time by the lidar and the other instruments on-board can be used for a meaningful comparison of the lidar parameters (color and depolarization ratios) with the aerosol concentration and size spectrum (Table 2). The CO mixing ratios are well correlated with the CPC data implying that combustion aerosols were often encountered with the largest concentrations at the end of the campaign. Changes in the pseudo color ratio PCR measured by the airborne lidar correspond quite well to the variations in aerosol mean diameter because R_{532} variations are small enough for these 10 layers to insure a weak dependency with the aerosol concentration (Fig. 3). The increase of CR_a from 0.2 to 0.35 is also in good agreement with the variation in the aerosol mean geometrical diameter if we exclude the cases with the largest error on CR_a. The uncertainty in the color ratios are calculated assuming a 30% and 15% relative uncertainty for the IR and green scattering ratio respectively. According to Table 2, the largest color ratios also correspond to the largest integrated GRIMM concentrations which are high for layers with coarse size aerosol. The PCR and CR_a values calculated by the airborne lidar can be then considered as valuable proxies for evaluating the contribution of the coarse aerosol fraction, and to first order (not considering speciation and

size) the lidar backscatter ratio is a good indicator of aerosol content.

2.3 Characterization of air mass transport

The origin of the air masses sampled during the aircraft campaign by the B-LNG lidar and by CALIOP was studied using the FLEXPART model version 8.23 (Stohl et al., 2002) driven by 6-hourly ECMWF analyses (T213L91) interleaved with operational forecasts every 3 hours. At a given location the model was run to perform domain filling calculations in 13 boxes from 1- to 7.5-km altitude with a horizontal dimension of 1°x 1°. The transport from the different regions are considered for two altitude ranges: < 3 km and between 3 and 7 km in order to distinguish the two major transport pathways to the Arctic: low level flow over cold surfaces, upper level advection by ~~an~~ uplifting along the tilted isentropes (Fuelberg et al., 2010; Stohl et al., 2006). This was done along the 18 aircraft cross sections and the 80 CALIPSO tracks in the European Arctic domain shown in Fig.1. For each box, 2000 particles were released during 60 minutes and the dispersion computed for 6 days backward in time. Longer simulations lead to larger uncertainties in the source attribution and are not considered in this work. We have introduced in the FLEXPART model the calculation of the fraction of particles originating below the 3 km altitude level for 3 areas with continental emissions shown in Fig.4 (Europe, Eurasia, North America). We have also calculated the fraction of particles present at latitudes above 70°N in the troposphere above the eastern Arctic and western Arctic (black boxes in Fig.4). The use of the eastern Arctic fraction is necessary to identify the role of the Eurasian sources because with our limited simulation time (6 days), we underestimate the role of aged air masses related to Eurasian emissions (ADV2010).

The results first show negligible influence of the transport from the lower troposphere above North America and are not considered further here. The fraction of air mass origins for the other regions is shown for different latitude bins in Fig. 5. The meridional distribution and the relative influence of the different regions are rather similar for the CALIPSO tracks and the airborne lidar flights in the lower atmosphere. However in the mid-troposphere, the increase of the relative influence of the Eastern Arctic air versus European air masses is clearly shifted towards higher latitudes (74°N) for CALIOP (no contribution in the 71 °N -72°N latitude band

as seen for the airborne data). For both data set, the transport of air masses from the Eastern Arctic show a clear latitudinal increase in the lower altitude range just north of the polar front. For latitudes above 73°N, seen only by CALIOP, the overall influence of all the selected source regions on a time scale shorter than 6 days remains ~~however~~ smaller than 40% implying that a large fraction of air masses had stayed for more than 6 days in the European Arctic sector located between -15°W and 30°E. Dilution, mixing and decay of the aged mid-latitude sources are to be expected at these latitudes. The main differences between CALIOP and the airborne lidar sampling are (i) a significant contribution from Eurasian sources at low latitudes for the aircraft data (ii) a weaker contribution of the Eastern Arctic sector in the mid-troposphere for CALIOP, especially around 70-72 °N. For the airborne lidar, the Eurasian sources are not only transported into the Arctic above the Pacific western coast but also by a low level southerly flow over eastern Europe from 6 to 9 April 2008. These differences are most probably due to the much larger longitude band selected for the analysis of the CALIOP data set (5°W to 35°W) Despite these differences, the overall similarity of the transport regime for both data sets is a good indication that the small number of aircraft flights is fairly representative of the influence of the different source regions, and the data gathered may be used to compare retrieved aerosol properties in the campaign area.

3 Analysis of CALIOP data during the aircraft campaign

3.1 Methodology of the CALIOP data processing

A detailed description of the CALIOP operational processing can be found in a series of papers (Vaughan et al., 2009; Liu et al., 2009; Omar et al., 2009; Powell et al., 2009). Uncertainties in the AL2 color ratio and the depolarization ratio are often very large and they are mainly used for a qualitative analysis of the aerosol composition and evolution (see Omar et al. (2009) for interpretation of the color ratio and the depolarization ratio for aerosol classification). Most of the error in the color ratio finds its origin in the signal calibration. More recently, analyses have been conducted to improve the calibration in version 4 (Vaughan et al., 2012), that confirmed a

bias in the 1064 nm channel and to a small extent the one in the 532 nm daytime channel. We thus considered a comparison between airborne and spaceborne CALIOP L1 observations as a first step.

In ADV2010, the AL2 CALIOP products were analyzed for one particular flight of the POLARCAT campaign using layers detected at 80-km horizontal resolution and with a 3% threshold value for the layer optical depth at 532 nm. Comparisons between the CALIOP AL2 and airborne lidar PCR then showed larger values for CALIOP in the aerosol layers of the 11 April flight. Considering the large uncertainty in the weak aerosol layers detected in the AL2 product over the Arctic, averaging of the L1 version 3.01 CALIOP data are used in this paper to analyze the 45 CALIPSO tracks available in the aircraft campaign domain. The comparison of the aerosol parameter PDF obtained for the campaign period and the campaign area is considered as more appropriate to validate the satellite aerosol data than relying on optimized collocations of aircraft and satellite data, which would give a very small number of cases. Gridded latitudinal distributions with a 1.5^{o} resolution in the campaign area are used to check the coherency of the two data sets.

The CALIOP L1 attenuated backscatter coefficients β_{1064} and β_{532}, are available with ~~an~~ 333 m horizontal resolution up to the 8.2 km vertical level and ~~it is~~ 1 km at higher altitude. Before making any horizontal or vertical averaging of these data, it is necessary to apply a cloud mask on the L1 data set. This cloud mask is based on the cloud mask features available in the level 2 version 3.01 CALIOP cloud (CL2) data products for the 5-km horizontal resolution. Additional checks have however been added to verify that cloud layers are not misclassified. First, ice cloud layers, detected in the 80 km horizontal resolution profile, must have a pseudo color ratio > 0.6 and a layer depolarization ratio > 0.3. If this is not the case, the 3 brightness temperatures $T_{12\mu m}$, $T_{10\mu m}$, $T_{8\mu m}$ measured by the IR Imaging Radiometer (IIR) installed on the same platform (Garnier et al., 2012), are used as an additional test to keep the layer as a cloud layer or not. Based on simulations, the criteria to keep a layer as a cloud layer is that the differences $T_{8\mu m}$-$T_{12\mu m}$ and $T_{10\mu m}$-$T_{12\mu m}$ must be positive (Dubuisson et al., 2008). Second, if the cloud layer is also detected in the 333-m resolution CL2 data products, it is always kept as a cloud as explained in Liu et al. (2009). Only very dense aerosol layers (scattering ratio $>$

3) are misclassified when adding these two conditions.

The β_{1064} and β_{532} data are then removed below the highest cloud top altitude for each vertical profile, when the optical depth (OD) of the cloud is larger than 1. For semi-transparent clouds with smaller ODs (<0.9), a transmission correction is performed. The data are also excluded in the 100 m layer just above the cloud top to avoid any error in the cloud top estimate. The cloud filtering is then very conservative in order to exclude a possible bias in the aerosol parameters measured below clouds when the spectral variation of the overlaying cloud attenuation has to be taken into account.

The cloud filtered 333-m attenuated backscatter vertical profiles are then averaged horizontally over 80 km and vertically over 150 m with a low pass 2nd order polynomial filter to improve the signal to noise ratio. The 80-km mean attenuated backscatter ratio $R_{532}(z)$ and $R_{1064}(z)$, the mean aerosol color ratio, and the mean 532-nm volume depolarization ratio are finally calculated using the molecular density and ozone vertical profiles available at 33 standard altitudes in the CALIOP data products.

As explained before two different methods are used for the comparison with airborne lidar observations:

- PDF of aerosol parameters using all the 80 km, 150 m averaged profiles available in the aircraft campaign area, i.e. with 0<z<7 km, 65°N<latitude<72.5°N, 5°E < longitude < 35°E, from 27 March to 11 April 2008
- latitudinal cross section in the same campaign area where 80 km, 150 m averaged profiles are gridded into 5x14 boxes with a 1.5°latitude and 500 m vertical resolution.

3.2 Impact of the 1064 nm CALIOP calibration on the aerosol color ratio

Two $R_{532}(z)$ mean profiles out of the 1.5°gridded data set are compared with the corresponding $R_{1064}(z)$ mean profiles in Fig.6. The $R_{1064}(z)$ is scaled to $R_{532}(z)$ to facilitate the comparison, assuming two extreme values of the expected aerosol color ratio CR_a (0.5 and 1), the range of values proposed by Cattrall et al. (2005). This corresponds to factors of 8 and 16, respectively in the scaling of $R_{1064}(z)$-1. For both latitude bins, a good consistency is obtained between

the aerosol vertical structures at both wavelengths showing that the proposed averaging reduces the noise ~~at a level high enough~~ to detect the mean aerosol layering at 1064 nm. The layer at 8 km can be used to identify the appropriate aerosol color ratio because the spectral variation of the aerosol attenuation of the signal above the layer is not very important. With the lidar 1064 nm calibration factor used in the Version 3 CALIOP L1 data products (see top figures in Fig.6), the ratio between $R_{532}(z)$-1 and $R_{1064}(z)$-1 in this upper layer leads to CR_a near 1 for both examples. This would mean that large dust like aerosols contribute in both cases to the tropospheric aerosol in the European Arctic sector no matter which latitude band is chosen, which does not seem to be credible. Furthermore depolarization remains low ($< 5\%$).

The 1064 calibration in the Version 3 CALIOP data set is based on the assumption that for a specific set of cirrus clouds, the cloud color ratio is equal to 1 allowing the 532 nm calibration to be transfered to the 1064 channel. This is detailed in a large number of publications (Vaughan et al., 2010, 2012; Reagan et al., 2002; Winker et al., 2013). The cirrus cloud selection in Version 3 implies an altitude range between 8 and 17 km and a minimum scattering ratio (>50). The number of cirrus clouds with these characteristics are too small (<11) for the campaign domain and period and no additionnal check was performed to verify the cirrus color ratio.

To reconcile the aerosol color ratio with the expected value, 3 options are available: to decrease the 1064 total backscatter, to increase the 532 nm total backscatter, or to change both parameters. Considering the uncertainty of the 1064 nm channel (Vaughan et al., 2012) and the difficulty to estimate the respective impact of sampling differences and calibration error of the 532 nm CALIOP data (see section 3.3), the 532 nm total backscatter values were not adjusted to the airborne data. The choice was to apply instead an a priori fixed multiplicative factor on the 1064 nm total backscatter, assuming a 40% and 30% overestimate for daytime and nighttime conditions, respectively. For daytime this is estimated from the B-LNG mean scattering ratios (see Fig.2). A reduced value was considered for nighttime, as linked to the ratio in the daytime and nighttime scale factors in Version 3 CALIOP data as mentioned in previous analysis (Wu et al., 2011; Vaughan et al., 2012). The ratio between $R_{532}(z)$-1 and $R_{1064}(z)$-1 then becomes more realistic since it leads to CR_a intermediate between 0.5 and 1 for the upper layer near 8 km, but also for the layers in the lower troposphere.

To verify that large CR_a for uncorrected IR data is not related to a bias introduced by the averaging of many profiles before the calculation of the color ratio, we have looked at the $R_{532}(z)$ versus $R_{1064}(z)$ scatter plot using all the 80 km resolution CALIOP filtered data for the altitude ranges, 0-7 km and 13-15 km. The scatter plots are presented in Fig. 7 for the uncorrected and corrected IR data using a frequency contour plot. Since we expect a very weak aerosol contribution in the 13-15 km altitude range, no specific correlation are found between $R_{532}(z)$ versus $R_{1064}(z)$. The noise of the 532-nm attenuated backscatter is of the order of 0.15 x molecular backscatter while the noise of the 1064-nm attenuated backscatter is 3 and 4 x molecular backscatter with and without the correction of IR data, respectively. Accounting for the factor 16 between the two molecular contributions, the noise in the IR channel is only 1.2 larger than the 532-nm noise value when correcting the IR data. Such a ratio is comparable to the analysis of Wu et al. (2011) at 16 km for all the daytime CALIOP data. No correction of the IR would mean a ratio of 1.7 between the 532-nm and 1064-nm signal noise level. The overestimate of the 1064-nm backscatter is even more likely when looking at the scatter plot for the altitude range 0-7 km. The slope of the regression line is indeed too small for the uncorrected IR data since it corresponds to many CR_a values larger than 1. The frequency of clean air masses (R=1) is also more consistent between the 532-nm and the 1064-nm observations after the correction of the IR overestimation provided that the 532 nm scattering ratio is correct.

The impact on the cirrus color ratio was not evaluated for the small number of occurences in our domain but it would imply a positive bias of 40% when using the Version 3 calibration. Such a bias is larger that the uncertainty of $\pm$ 20-30% proposed for the 1064 nm calibration procedure (Wu et al., 2011; Vaughan et al., 2012). We must recall however that a 40% bias can be also accounted for if we assume a negative bias of 5% for the 532 nm scattering ratio. As explained in section 3.3, this hypothesis was not considered in this work and the re-calibration of the 1064 nm signal was chosen. It will be interesting to test this hypothesis using the new Version 4 level 1 Caliop data which will be available. In the new Version 4, the cirrus cloud selection for the 1064 calibration (i.e. with a cloud color ratio of 1) has been updated (cloud temperature instead of altitude selection, use of the cloud depolarization ratio) providing more cirrus clouds and better altitude selection for the Arctic (Vaughan et al., 2012).

3.3 Comparison of airborne lidar and CALIOP

3.3.1 Analysis of the statistical distribution

Using the dataset averaged over the campaign period/domain, the distributions of the CALIOP corrected R_{1064} and R_{532} are shown in Fig. 8 for the range 0-7 km and 13-15 km. The latter corresponds to very low aerosol concentrations. It has a mean and a median with a difference less than 0.02 at 532 nm and 0.3 at 1064 nm from the expected scattering ratio of 1. The large standard deviations of 0.3 at 532 nm and 4 at 1064 nm is expected at this altitude level where the molecular backscatter decreases significantly.

The $\overline{R_{1064}}$ mean (2.3) is close to the airborne lidar value (2.1) considering an error of the mean of the order of 0.1 and even though the standard deviation of the noisy CALIOP R_{1064} distribution is 1.7 times larger than the airborne lidar corresponding value. The same ratio is observed between the airborne and CALIOP R_{532} standard deviation. Therefore, this confirms the validity of the estimated correction factor, although with a large statistical error (about 30% on the coefficients) for the 1064 nm CALIOP profiles selected in our study of the Arctic region.

Contrary to the airborne lidar distribution, the CALIOP R_{532} distribution in the troposphere below 7 km does not show many layers with elevated aerosol concentrations as shown by a lower value of the 90th percentile (1.34 for CALIOP instead of 1.45 for the airborne lidar). The larger standard deviation (0.34 instead of 0.2) is related to the poorer signal to noise ratio of the satellite dataset. The lower value for the 532 nm mean (1.13 instead of 1.21) is larger than the expected uncertainty on the mean of the CALIOP distribution which is of the order of 0.01. This uncertainty of the mean is calculated assuming an error of 0.4 for a single CALIOP measurement (i.e. the width of the distribution for the negative values) and assuming 1700 independent layers out of 28872 data points available in the 0 and 7 km altitude range above the campaign domain (i.e. considering a 1 km vertical sampling instead of the 60 m vertical resolution to ensure independence). Since we compare patchy data, it is also important to assess how the averaging of aerosol layers with observed clear air scenes may explain this difference. For example, the difference between the airborne and CALIOP $\overline{R_{532}}$ averages can be explained if there are twice as many layers with low aerosol load ($R_{532} < 1.05$) in the CALIOP data set.

This may be related to the fact that in our CALIOP data processing we remove all the total backscatter values below clouds. It is also necessary to check whether this difference may also be due to (1) an overestimate of the 532 nm CALIOP calibration factor (2) an underestimate of the airborne lidar calibration factor. Positive differences due to 532 nm daytime calibration uncertainty were also obtained by (Rogers et al., 2011) when comparing NASA HSRL airborne lidar and CALIOP data for measurements at high latitudes in the Northern Hemisphere, but the mean difference is not higher than 3%. The remaining 5% uncertainty on the mean difference can be accounted by a systematic error in the airborne lidar calibration when assuming no aerosol in the altitude range which corresponds to the smallest attenuated backscatter coefficient. Comparisons with other observations confirmed that 532 nm CALIOP data could be underestimated by about 5%, due to the occurrence of residual stratospheric aerosols at the normalization altitude (Vernier et al., 2009). This would be supported by the fact that we obtain a very small value (<2%) of the 532 nm mean aerosol scattering ratio in the 13-15 km range when using the Version 3.0 calibration.

The average $\overline{CR_a}$ is 0.44±0.8 for CALIOP ~~which~~ is not very far from the airborne lidar value (0.31±0.12) considering the factor of 6 between the two standard deviations of this parameter (Fig. 8). For the noisy satellite data, a better proxy is $\overline{CR_a}^*$=0.65±0.1, i.e. the mean color ratio calculated with ($\overline{R_{532}}$-1) and ($\overline{R_{1064}}$-1), which is then 2 times larger than the similar ratio for the airborne lidar. This can be explained by the 10% bias in $\overline{R_{532}}$ which are always less than 1.35. Therefore this difference cannot be interpreted as a stronger contribution of the coarse size aerosol fraction in the satellite observations. Despite this bias in the order of magnitude of $\overline{CR_a}^*$, it is important to verify if the relative spatial or temporal variability is detected by the satellite data.

3.3.2 Analysis of the latitudinal distribution

The latitudinal variability of the aerosol properties is studied using the CALIOP latitudinal grid data set described earlier, i.e. considering 5 successive 1.5 °latitude bins and 14 vertical layers of 500 m. The airborne lidar data are analyzed only for layers where the aerosol content is high enough to be observed in the 1064 nm profiles. There are 90 well defined and independent

aerosol layers identified in the 18 lidar cross sections at latitudes less than 72.5°N. For the campaign period, we do not have many data below 1 km (see Fig.3 in supplementary information document), so the comparison of the latitudinal variations is made for the two following altitude ranges: 1-3 km and 3-7 km. The latitudinal distributions of R_{532}, CR_a and δ_{532} (or δ_{355}) are shown for both data sets in Figs. 9 and 10. For each aerosol layer, the FLEXPART analysis was used to distinguish between European or Eurasian air masses transported by the southerly flow on one hand, and the Eurasian or North American sources advected in our domain through the polar dome on the other hand. The green and red data points correspond to Eastern Arctic and Western Arctic origins, respectively, while the black points indicate the influence of mid latitude sources directly advected by the southerly flow. Each point in the airborne lidar plots corresponds to a single layer observed by the aircraft, while for CALIOP it corresponds to an average of several layers at the same altitude in the selected latitude band.

Lower troposphere (< 3 km)

For the lower troposphere (Fig.9), the airborne lidar does not show a clear latitudinal dependency of the aerosol scattering ratios for the Eastern Arctic and European/Eurasian sources. A decrease of the occurrence of elevated aerosol concentrations is however observed by CALIOP at the lowest latitudes. This is especially true for the Eastern Arctic aerosol type. The increase of cloudiness at southern latitudes may explain this evolution because of the lower probability of observations in the lowermost troposphere. The significant number of CALIOP R_{532} values below 1.1 identified in the statistical analysis discussed in the previous section is seen at all latitudes. Although the range of CR_a are larger for CALIOP (0.6-1.1 instead of 0.2-0.5 for the airborne lidar), the relative latitudinal variations are somewhat similar with a maximum between 70°N and 72°N, especially when focusing on the Eastern Arctic air masses.

The δ_{355} values measured by the airborne lidar are less than 1.5% for no depolarization and exceed 2% when depolarization is present, while the uncertainty is of the order of 0.2%.Values of δ_{532} measured by CALIOP are larger ranging from 3% to 11%, because of a spectral variation of the aerosol depolarization ratio. Assuming a backscatter ratio of the order of 1.1 at 355 nm and 1.3 at 532 nm, such a change of PDR correspond to a change of the aerosol depolar-

ization ratio from 5% at 355 nm to 10% at 532 nm. Such a spectral variation was observed by Gross et al. (2012) in a mixture of volcanic ash and marine aerosol when hygroscopic aerosol was present but at[illegible] small enough to decrease only the 355 parallel backscatter. A similar kind of mixture could exist in our European Arctic domain and was found in aircraft measurements over Alaska in April 2008 (Brock et al., 2011). Regarding the latitudinal increase of the depolarization ratio, it is seen for both data sets.

Mid-troposphere (>3 km)

For the mid-troposphere (Fig.10), the latitudinal decrease of the backscatter ratio is observed in the airborne and the CALIOP lidar data, especially for the southerly flow. The CALIOP observations are never strongly related to [illegible]astern Arctic at latitudes less than 75°N for the altitudes above 3 km as discussed in section 2.3. So the comparison is only meaningful when considering the air masses advected by the southerly flow. For both data set, the latitudinal variations are consistent: a small increase of CR_a, a decrease of the pseudo depolarization ratio.

To conclude, there are significant differences in the magnitude of CR_a (mainly related to differences in the magnitude of R_{532}) and in the magnitude of the depolarization ratio (related to the expected spectral variation between 532 and 355 nm), but the spatial variations are rather similar for both datasets considering the limited coverage of the airborne data. The comparison of the R_{532} 1.5°averaged vertical profiles is also useful to discuss the relative influence of calibration error and sampling differences between CALIOP and the B-LNG airborne lidar (Fig. 11). For the altitude ranges with the largest aerosol content (below 2 km and above 4 km), the order of magnitude of R_{532} is similar and varies in the same direction when increasing the latitude bin. The largest differences are in the 1.5 to 4 km altitude range corresponding to the lowest values of R_{532} where the CALIOP data are frequently below 1.1. Therefore, the bias in R_{532} is not only related to calibration issues, but also to the fact that the airborne lidar saw more air masses with significant aerosol content in the altitude range 1.5 to 4 km. This may be related to the specific targeting of the aircraft flights to sample such layers and also to the fact that many of these layers are observed below 4 km in the frontal zone where overlying clouds (see

supplementary document) make the detection by the CALIOP overpasses more difficult. The wider longitude range chosen for the CALIOP data set do not compensate for this difference in the observed air masses. Since the difference in the magnitude of the 532 nm backscatter ratio is not only related to a calibration uncertainty in one instrument or both, but also to differences in the number of observations with low aerosol content in the altitude range 1.5 to 4 km, we choose not to apply any correction to the 532 nm CALIOP data set.

4 CALIOP characterization of the aerosol layer properties in April 2008

4.1 Latitudinal variability in the European Arctic

In this section, the CALIOP data are now analyzed for 30 days in April 2008 to improve further the signal-to-noise ratio. The latitudinal distribution of aerosol properties in the European Arctic is still derived using average CALIOP vertical profiles for 1.5 ^{o}latitude bins, but over a larger domain between 65^{o}N and 80^{o}N. Two specific altitude ranges (0-2 km and 5-7 km) have been selected because they correspond to the largest aerosol load identified in the mean vertical profile over the European Arctic (Fig.11).

Lower troposphere (0-2 km)

In the lower troposphere, the meridional cross section of R_{532} reveals that the largest aerosol scattering in the PBL is for the eastern Arctic origin and mainly in the Arctic frontal zone between 69^{o}N and 75^{o}N (Fig. 12). The large error bars corresponding to small aerosol loads encountered in the Arctic, limit the quantitative analysis of the CR_a meridional distribution. The slight increase of CR_a with latitude is mainly related to the variation of CR_a with the air mass origin. The eastern Arctic aerosol layers show $CR_a > 1$ while air masses with a European origin correspond to $CR_a \approx 0.7$. The δ_{532} cross section shows significant depolarization (near 10% for the monthly average) within the 70^{o}N - 73^{o}N latitude range. Considering the high scattering ratios, the significant fraction of coarse size aerosol (CR_a near 1) and the depolarization, a contribution of ice crystal formation in the frontal zone is very likely in this latitude range.

When excluding these specific cases, the European aerosol layers have larger depolarization than eastern Arctic air masses. Larger and more spherical aerosols for the eastern Arctic layers is not so surprising considering aerosol aging in air masses transported from Asia (Massling et al., 2007).

Mid-troposphere (5-7 km)

In the mid troposphere (5-7km), there is a general decrease in R_{532} with latitude for the European air masses, while it increases for the eastern Arctic origin. So in contrast to the PBL there is a minimum of aerosol contribution near 72°N. This can be explained if one assumes a significant wet removal of particles during upward vertical transport within the Arctic front. As observed for the lower troposphere, CR_a values are lower for European air masses (near 0.5) than for Asian Arctic origin (near 0.8). We do not see the large depolarization values related to the possible presence of ice crystals above 5 km, since they are not transported out of the PBL. However the meridional distribution of the depolarization shows a clear decrease at the highest latitudes. The latitudinal increase of CR_a associated with a decrease in depolarization could be explained by the increasing importance of aged anthropogenic aerosol and not to a strong influence of dust particles. The in-situ analysis of the size distribution made in Quennehen et al. (2012) indeed showed, that Asian anthropogenic aerosol contributed significantly to the accumulation mode.

4.2 Large scale distribution in the Arctic domain

April monthly averages for R_{532}, CR_a and δ_{532} have been calculated for the complete Arctic domain (latitude $>$ 60°N) in horizontal boxes of 300 km x 300 km. The CR_a values are only given when R_{532} >1.25 to focus on the contribution of significant aerosol plumes, and to avoid large errors in CR_a due to small scattering ratios. The fraction of CALIOP observations available (i.e. not below a cloud) in the selected altitude range is also given to estimate the number of effective CALIOP tracks in every box. According to Fig.1 a minimum number of 10 overpasses is needed for the data to be representative of a monthly mean. This corresponds to a fraction of 50% at 65°N and 20% at 80°N.

Lower troposphere (0-2 km)

In the lower troposphere (Fig. 13), the R_{532} map shows the extent of a North Atlantic aerosol contribution with values remaining larger than 1.5 above 70°N. Sea salt and sulfate aerosol are known to contribute to the increase of aerosol scattering over the Atlantic in winter and early spring (Smirnov et al., 2000; Yoon et al., 2007). The CR_a map indicates a gradual increase of CR_a with latitude over North Atlantic: values < 0.7 occur near the mid-latitude sources located below 65°N but $CR_a > 0.9$ are frequent above 70°N. The latitudinal gradient of CR_a over the North Atlantic ocean can be related to the growing influence of a different kind of aerosol, since the probability of aerosol particle transport from the Eastern Arctic is increasing as discussed in the previous section. Aerosol composition analysis onboard the NOAA ship during the ICEALOT campaign (Frossard et al., 2011) have shown that marine and sulfate aerosol represent 70% of the submicronic aerosol composition in the North Atlantic east of Iceland and they also found that the sulfate contribution increases with latitude. This is broadly consistent with the CALIOP observations.

A local maximum in the R_{532} map is also observed over Siberia between 90°E and 110°E with a latitudinal extent up to 70°N in the Taymir peninsula. In Spring 2008 this area is known to be influenced on one hand by local anthropogenic emissions from gas flaring (Stohl et al., 2013), and on the other hand by early spring forest fires in Russia (Warneke et al., 2010). The maximum in Northern Siberia is also seen for the same area in the AOD analysis made by Winker et al. (2013) using CALIOP data for the winter period before the fire period, then implying a significant contribution of anthropogenic emissions. The CR_a values < 0.7 are similar to those observed below 65°N over the Atlantic ocean. No significant depolarization is observed in these two source regions implying very little impact from dust or volcano emissions in this altitude range. The difference of CR_a between European Arctic and the source region in Russia implies a growing of the aerosol particles during transport and aging if one assumes that most of the aerosol layers observed in European Arctic originate from Eurasia (see previous section).

Mid-troposphere (5-7 km)

In the mid-troposphere (Fig. 14), the R_{532} map gives a very different picture of the link between the Arctic aerosol distribution and the mid-latitude sources. There is first a broad aerosol maximum from eastern Siberia to western Alaska at latitudes between 60 ^{o}N and 75^{o}N and second another maximum over the Hudson bay. The eastern Arctic domain north of 70^{o}N is not as clean as in the lower troposphere, being consistent with an efficient transport pathway from mid-latitudes along the tilted isentropic surfaces (Harrigan et al., 2011). The western Arctic and North Atlantic are relatively free of aerosol particles in the mid-troposphere. This is somewhat contradictory with the known uplift of the low level North American air pollution over western Greenland (Harrigan et al., 2011; Ravetta et al., 2007). The contrast between the large aerosol concentrations found in the North Atlantic lower troposphere and the low values above is also consistent with the conclusion of several papers (Law and Stohl, 2007; Harrigan et al., 2011) about the transport pathway of European emission being most efficient in the lower troposphere.

The global cloud distribution can be obtained from the DARDAR products, which are based on CloudSat and CALIOP data according to a variational scheme, on a 60 m vertical resolution and 1 km horizontal resolution grid (Delanoë and Hogan, 2008). The synergy between lidar and radar is indeed needed to have a detailed picture of the cloud vertical profile (Ceccaldi et al., 2013). It has been used here to calculate the cloud fraction at different altitudes during the month of April 2008 in 4 different latitude bands from 60^{o}N to 80^{o}N (Fig. 15). The latitudes with large cloudiness in both the mid and upper troposphere show upward frontal lifting by Warm Conveyor Belts (WCB) near the Bering strait and the western Greenland coast. The latter shows the largest cloudiness at 5 km. This may explain the low aerosol concentration downwind of Greenland due to efficient removal of aerosol. One can also notice the good correlation between the high values of the low level cloud fraction and the large aerosol load observed above 70^{o}N in the European Arctic.

The aerosol depolarization and color ratio distributions show small and little depolarization (except over the Hudson bay) in the large scale aerosol plumes seen in the mid-troposphere. However as in the lower troposphere, the CR_a increase at latitudes $>$70^{o}N is consistent with aerosol aging when reaching the highest latitudes.

5 Conclusions

In this paper we have analyzed aerosol airborne (B-LNG) and spaceborne (CALIOP) lidar data related to the transport of mid-latitude sources into the Arctic. The main results are the following:

- A campaign was held in April 2008 in the European Arctic with 18 aircraft cross sections and 80 CALIPSO tracks over 15 days improving our ability to identify the transport of aerosol layers to the Arctic, especially from the analysis of the satellite data.

- Analysis of the B-LNG backscatter ratio R_{532} and R_{1064} at two wavelengths for the calculation of the aerosol color ratio (CR_a) has been successfully compared with in-situ aerosol measurements on-board the aircraft. The CR_a increase corresponds to a similar increase in the mean aerosol diameter, showing the importance of multi-wavelength analysis. It also emphasizes the need for accurate lidar calibration.

- Simulations with the FLEXPART model show that the limited number of airborne lidar cross sections are representative of the main characteristics of the air mass transport in April 2008: increase with latitude of the aged air masses from the Eastern Arctic region at altitude level below 3 km, large influence of the mid-latitudes sources directly transported by the southerly flow at altitudes above 3 km.

- Comparisons are performed between B-LNG and CALIOP backscatter ratio R_{532} and R_{1064} at two wavelengths, including the calculation of the aerosol color ratio and of the depolarization ratio (PDR) at 532 nm or 355 nm. Comparisons are based on the analysis of 15 day averages and L1 CALIOP data processing instead of AL2 CALIOP operational products. Specific averaging methods can then be applied. The cloud screening, needed when using L1 lidar data, is based on CL2 CALIOP data products and the IR CALIPSO radiometer data. A re-calibration of the CALIOP R_{1064} in the Arctic was chosen to reduce the positive bias of the CALIOP data with respect to airborne observations of the color ratio. A fixed factor was applied to the 1064 nm attenuated backscatter data, of 1.3 and

1.4, respectively, for nighttime and daytime orbits. This value could be significatively smaller if a small negative bias of the 532 nm CALIOP lidar signal is also corrected, but this hypothesis was not applied in this work. The use of the new Version4.0 data which will be available very soon would certainly help to address this question.

– Comparisons of the statistical distributions in the altitude range 0-7 km show no significant bias for R_{1064} when correcting the CALIOP 1064 nm data but a -8% negative difference between the CALIOP and B-LNG R_{532} data. The latter might be related to a calibration problem of either the B-LNG or the CALIOP instrument. However the differences being largest in a specific altitude range between 1.5 and 4 km, differences of the spatial averaging of airborne and satellite data are also to be considered. The difference in the magnitude of CR_a is mainly related to this overestimate of R_{532} in the B-LNG data. The depolarization ratio is not measured at the same wavelength and its spectral variation follows that of hygroscopic aerosol often at a size small enough to be detected only at 355 nm (Gross et al., 2012).

– The latitudinal distribution of the color ratio and the depolarization ratio is similar for the B-LNG and the CALIOP data sets, especially considering the limited number of aircraft flights. It is a good indication that, despite possible bias in these two parameters when comparing airborne and satellite data, they are still valuable for the analysis of the aerosol growth or the relative fraction of dust or volcanic ashes using CALIOP observations.

– The monthly average analysis of the CALIOP color and depolarization ratio in the European Arctic area show that larger (higher CR_a) and more spherical aerosol (low PDR) are expected in the air masses transported from the Eastern Arctic both in the lower troposphere (0-2 km) and in the mid troposphere (5-7 km). Less aerosol is present in the mid troposphere near the arctic front (70°N-74°N) while significant R_{532} and depolarization ratio are seen in the lower troposphere possibly related to the presence of ice crystal.

– The global distribution of the CALIOP monthly analysis reveal two regions with large backscatter below 2 km: the Northern Atlantic between Greenland and Norway, and the

Taymir peninsula. The CR_a increase between the source regions and the observations at latitudes above 70°N implies a growth of the aerosol size once transported to the Arctic. The distribution of the aerosol optical properties in the mid troposphere is consistent with the transport pathways proposed in Harrigan et al. (2011): (i) low level advection in Northern Europe (ii) isentropic uplifting of pollution and biomass burning aerosol in Northern Siberia and Eastern Asia, (iii) aerosol washout by the North Atlantic warm conveyor belts.

Acknowledgements. The UMS SAFIRE is acknowledged for supporting the ATR-42 aircraft deployment and for providing the aircraft meteorological data. The POLARCAT-FRANCE and CLIMSLIP projects were funded by ANR, CNES, CNRS/INSU and IPEV. The FLEXPART team (A. Stohl, P. Seibert, A. Frank, G. Wotawa, C. Forster, S. Eckhardt, J. Burkhart, H. Sodemann) is acknowledged for providing the FLEXPART code. NASA, CNES, the ICARE and LARC data center are gratefully acknowledge for supplying the CALIPSO data.

References

Adam de Villiers, R., Ancellet, G., Pelon, J., Quennehen, B., Schwarzenboeck, A., Gayet, J. F., and Law, K. S.: Airborne measurements of aerosol optical properties related to early spring transport of mid-latitude sources into the Arctic, Atmospheric Chemistry and Physics, 10, 5011–5030, doi: 10.5194/acp-10-5011-2010, http://www.atmos-chem-phys.net/10/5011/2010/, 2010.

Brock, C. A., Cozic, J., Bahreini, R., Froyd, K. D., Middlebrook, A. M., McComiskey, A., Brioude, J., Cooper, O. R., Stohl, A., Aikin, K. C., de Gouw, J. A., Fahey, D. W., Ferrare, R. A., Gao, R.-S., Gore, W., Holloway, J. S., Hübler, G., Jefferson, A., Lack, D. A., Lance, S., Moore, R. H., Murphy, D. M., Nenes, A., Novelli, P. C., Nowak, J. B., Ogren, J. A., Peischl, J., Pierce, R. B., Pilewskie, P., Quinn, P. K., Ryerson, T. B., Schmidt, K. S., Schwarz, J. P., Sodemann, H., Spackman, J. R., Stark, H., Thomson, D. S., Thornberry, T., Veres, P., Watts, L. A., Warneke, C., and Wollny, A. G.: Characteristics, sources, and transport of aerosols measured in spring 2008 during the aerosol, radiation, and cloud processes affecting Arctic Climate (ARCPAC) Project, Atmospheric Chemistry and Physics, 11, 2423–2453, doi:10.5194/acp-11-2423-2011, http://www.atmos-chem-phys.net/11/2423/2011/, 2011.

Burton, S. P., Ferrare, R. A., Hostetler, C. A., Hair, J. W., Rogers, R. R., Obland, M. D., Butler, C. F., Cook, A. L., Harper, D. B., and Froyd, K. D.: Aerosol classification using airborne High Spectral

Resolution Lidar measurements - methodology and examples, Atmospheric Measurement Techniques, 5, 73–98, doi:10.5194/amt-5-73-2012, http://www.atmos-meas-tech.net/5/73/2012/, 2012.

Cattrall, C., Reagan, J., Thome, K., and Dubovik, O.: Variability of aerosol and spectral lidar and backscatter and extinction ratios of key aerosol types derived from selected Aerosol Robotic Network locations, J. Geophys. Res., 110, D10S11, doi:10.1029/2004JD005124, 2005.

Ceccaldi, M., Delanoë, J., Hogan, R. J., Pounder, N. L., Protat, A., and Pelon, J.: From CloudSat-CALIPSO to EarthCare: Evolution of the DARDAR cloud classification and its comparison to airborne radar-lidar observations, Journal of Geophysical Research: Atmospheres, 118, 7962–7981, doi:10.1002/jgrd.50579, http://dx.doi.org/10.1002/jgrd.50579, 2013.

Delanoë, J. and Hogan, R. J.: A variational scheme for retrieving ice cloud properties from combined radar, lidar, and infrared radiometer, J. Geophys. Res., 113, D07 204, doi:10.1029/2007JD009000, 2008.

Devasthale, A., Tjernstrm, M., Karlsson, K.-G., Thomas, M. A., Jones, C., Sedlar, J., and Omar, A. H.: The vertical distribution of thin features over the Arctic analysed from CALIPSO observations, Tellus B, 63, 77–85, doi:10.1111/j.1600-0889.2010.00516.x, http://dx.doi.org/10.1111/j.1600-0889.2010.00516.x, 2011.

Di Pierro, M., Jaeglé, L., Eloranta, E. W., and Sharma, S.: Spatial and seasonal distribution of Arctic aerosols observed by CALIOP (2006-2012), Atmospheric Chemistry and Physics Discussions, 13, 4863–4915, doi:10.5194/acpd-13-4863-2013, http://www.atmos-chem-phys-discuss.net/13/4863/2013/, 2013.

Dubuisson, P., Giraud, V., Pelon, J., Cadet, B., and Yang, P.: Sensitivity of Thermal Infrared Radiation at the Top of the Atmosphere and the Surface to Ice Cloud Microphysics, Journal of Applied Meteorology and Climatology, 47, 2545–2560, doi:10.1175/2008JAMC1805.1, http://dx.doi.org/10.1175/2008JAMC1805.1, 2008.

Freudenthaler, V., Esselborn, M., Wiegner, M., Heese, B., Tesche, M., Ansmann, A., Müller, D., Althausen, D., Wirth, M., Fix, A., Ehret, G., Knippertz, P., Toledano, C., Gasteiger, J., Garhammer, M., and Seefeldner, M.: Depolarization ratio profiling at several wavelengths in pure Saharan dust during SAMUM 2006, Tellus, 61B, 165–179, doi:10.1111/j.1600-0889.2008.00396.x, http://dx.doi.org/10.1111/j.1600-0889.2008.00396.x, 2009.

Frossard, A. A., Shaw, P. M., Russell, L. M., Kroll, J. H., Canagaratna, M. R., Worsnop, D. R., Quinn, P. K., and Bates, T. S.: Springtime Arctic haze contributions of submicron organic particles from European and Asian combustion sources, Journal of Geophysical Research: Atmospheres, 116, DO5205, doi:10.1029/2010JD015178, http://dx.doi.org/10.1029/2010JD015178, 2011.

Fuelberg, H. E., Harrigan, D. L., and Sessions, W.: A meteorological overview of the ARCTAS 2008 mission, Atmospheric Chemistry and Physics, 10, 817–842, doi:10.5194/acp-10-817-2010, http://www.atmos-chem-phys.net/10/817/2010/, 2010.

Garnier, A., Pelon, J., Dubuisson, P., Faivre, M., Chomette, O., Pascal, N., and Kratz, D. P.: Retrieval of cloud properties using CALIPSO Imaging Infrared Radiometer. Part I: effective emissivity and optical depth, Journal of Applied Meteorology and Climatology, 51, 1407–1425, doi:10.1175/JAMC-D-11-0220.1, 2012.

Garrett, T. and Zhao, C.: Increased Arctic cloud longwave emissivity associated with pollution from mid-latitudes, Nature, 440, 787–789, 2006.

Gross, S., Freudenthaler, V., Wiegner, M., Gasteiger, J., Geiss, A., and Schnell, F.: Dual-wavelength linear depolarization ratio of volcanic aerosols: Lidar measurements of the Eyjafjallajkull plume over Maisach, Germany, Atmospheric Environment, 48, 85 – 96, doi:10.1016/j.atmosenv.2011.06.017, http://www.sciencedirect.com/science/article/pii/S1352231011006108, 2012.

Harrigan, D. L., Fuelberg, H. E., Simpson, I. J., Blake, D. R., Carmichael, G. R., and Diskin, G. S.: Anthropogenic emissions during Arctas-A: mean transport characteristics and regional case studies, Atmospheric Chemistry and Physics, 11, 8677–8701, doi:10.5194/acp-11-8677-2011, http://www.atmos-chem-phys.net/11/8677/2011/, 2011.

Jacob, D. J., Crawford, J. H., Maring, H., Clarke, A. D., Dibb, J. E., Emmons, L. K., Ferrare, R. A., Hostetler, C. A., Russell, P. B., Singh, H. B., Thompson, A. M., Shaw, G. E., McCauley, E., Pederson, J. R., and Fisher, J. A.: The Arctic Research of the Composition of the Troposphere from Aircraft and Satellites (ARCTAS) mission: design, execution, and first results, Atmospheric Chemistry and Physics, 10, 5191–5212, doi:10.5194/acp-10-5191-2010, http://www.atmos-chem-phys.net/10/5191/2010/, 2010.

Law, K. and Stohl, A.: Arctic Air Pollution: Origins and Impacts, Science, 315(5818), 1537–1540, doi 10.1126/science.1137 695, 2007.

Liu, Z., Vaughan, M., Winker, D., Kittaka, C., Getzewich, B., Kuehn, R., Omar, A., Powell, K., Trepte, C., and Hostetlerd, C.: The CALIPSO Lidar Cloud and Aerosol Discrimination: Version 2 Algorithm and Initial Assessment of Performance, J. Atmos. Ocean. Tech., 26, 1198–1213, doi:10.1175/2009JTECHA1229.1, 2009.

Massling, A., Leinert, S., Wiedensohler, A., and Covert, D.: Hygroscopic growth of sub-micrometer and one-micrometer aerosol particles measured during ACE-Asia, Atmospheric Chemistry and Physics, 7, 3249–3259, doi:10.5194/acp-7-3249-2007, http://www.atmos-chem-phys.net/7/3249/2007/, 2007.

Omar, A., Winker, D., Kittaka, C., Vaughan, M., Liu, Z., Hu, Y., Trepte, C., Rogers, R., Ferrare, R.,

Lee, K., Kuehn, R., and Hostetler, C.: The CALIPSO Automated Aerosol Classification and Lidar Ratio Selection Algorithm, J. Atmos. Ocean. Tech., 26, 1994–2014, doi:10.1175/2009JTECHA1231.1, 2009.

Powell, K. A., Hostetler, C. A., Vaughan, M. A., Lee, K.-P., Trepte, C. R., Rogers, R. R., Winker, D. M., Liu, Z., Kuehn, R. E., Hunt, W. H., and Young, S. A.: CALIPSO Lidar Calibration Algorithms. Part I: Nighttime 532-nm Parallel Channel and 532-nm Perpendicular Channel, J. Atmos. Oceanic Technol., 26, 2015–2033, doi:10.1175/2009JTECHA1242.1, http://dx.doi.org/10.1175/2009JTECHA1242.1, 2009.

Quennehen, B., Schwarzenboeck, A., Matsuki, A., Burkhart, J. F., Stohl, A., Ancellet, G., and Law, K. S.: Anthropogenic and forest fire pollution aerosol transported to the Arctic: observations from the POLARCAT-France spring campaign, Atmospheric Chemistry and Physics, 12, 6437–6454, doi:10.5194/acp-12-6437-2012, http://www.atmos-chem-phys.net/12/6437/2012/, 2012.

Quinn, P. K., Bates, T. S., Baum, E., Doubleday, N., Fiore, A. M., Flanner, M., Fridlind, A., Garrett, T. J., Koch, D., Menon, S., Shindell, D., Stohl, A., and Warren, S. G.: Short-lived pollutants in the Arctic: their climate impact and possible mitigation strategies, Atmospheric Chemistry and Physics, 8, 1723–1735, http://www.atmos-chem-phys.net/8/1723/2008/, 2008.

Rahn, K. A.: Relative importances of North America and Eurasia as sources of arctic aerosol, Atmospheric Environment, 15, 1447 – 1455, doi:10.1016/0004-6981(81)90351-6, 1981.

Ravetta, F., Ancellet, G., Colette, A., and Schlager, H.: Long Range Transport and Tropospheric Ozone Variability in Western Mediterranean Region during ITOP2004, J. Geophys. Res., 12, D10S46, doi:10.1029/2006JD007724, 2007.

Reagan, J., Wang, X., and Osborn, M. T.: Spaceborne lidar calibration from cirrus and molecular backscatter returns, Geoscience and Remote Sensing, IEEE Transactions on, 40, 2285–2290, doi:10.1109/TGRS.2002.802464, 2002.

Rodríguez, E., Toledano, C., Cachorro, V. E., Ortiz, P., Stebel, K., Berjón, A., Blindheim, S., Gausa, M., and de Frutos, A. M.: Aerosol characterization at the sub-Arctic site Andenes (69°N, 16°E), by the analysis of columnar optical properties, Quarterly Journal of the Royal Meteorological Society, 138, 471–482, doi:10.1002/qj.921, http://dx.doi.org/10.1002/qj.921, 2012.

Rogers, R. R., Hostetler, C. A., Hair, J. W., Ferrare, R. A., Liu, Z., Obland, M. D., Harper, D. B., Cook, A. L., Powell, K. A., Vaughan, M. A., and Winker, D. M.: Assessment of the CALIPSO Lidar 532 nm attenuated backscatter calibration using the NASA LaRC airborne High Spectral Resolution Lidar, Atmospheric Chemistry and Physics, 11, 1295–1311, doi:10.5194/acp-11-1295-2011, http://www.atmos-chem-phys.net/11/1295/2011/, 2011.

Shinozuka, Y., Redemann, J., Livingston, J. M., Russell, P. B., Clarke, A. D., Howell, S. G., Freitag, S., O'Neill, N. T., Reid, E. A., Johnson, R., Ramachandran, S., McNaughton, C. S., Kapustin, V. N., Brekhovskikh, V., Holben, B. N., and McArthur, L. J. B.: Airborne observation of aerosol optical depth during ARCTAS: vertical profiles, inter-comparison and fine-mode fraction, Atmospheric Chemistry and Physics, 11, 3673–3688, doi:10.5194/acp-11-3673-2011, http://www.atmos-chem-phys.net/11/3673/2011/, 2011.

Smirnov, A., Holben, B. N., Kaufman, Y. J., Dubovik, O., Eck, T. F., Slutsker, I., Pietras, C., and Halthore, R. N.: Optical Properties of Atmospheric Aerosol in Maritime Environments, Journal of the Atmospheric Sciences, 59, 501–523, doi:10.1175/1520-0469(2002)059⟨0501:OPOAAI⟩2.0.CO;2, http://dx.doi.org/10.1175/1520-0469(2002)059⟨0501:OPOAAI⟩2.0.CO;2, 2000.

Stock, M., Ritter, C., Herber, A., von Hoyningen-Huene, W., Baibakov, K., Grser, J., Orgis, T., Treffeisen, R., Zinoviev, N., Makshtas, A., and Dethloff, K.: Springtime Arctic aerosol: Smoke versus haze, a case study for March 2008, Atmospheric Environment, 52, 48–55, doi:10.1016/j.atmosenv.2011.06.051, http://www.sciencedirect.com/science/article/pii/S1352231011006637, 2011.

Stohl, A., Eckhardt, S., Forster, C., James, P., Spichtinger, N., and Seibert, P.: A replacement for simple back trajectory calculations in the interpretation of atmospheric trace substance measurements, Atmospheric Environment, 36, 4635 – 4648, doi:10.1016/S1352-2310(02)00416-8, http://www.sciencedirect.com/science/article/B6VH3-46PBJBX-8/2/7d8c7b6557524176d31e8d96169cd1df, 2002.

Stohl, A., Andrews, E., Burkhart, J. F., Forster, C., Herber, A., Hoch, S. W., Kowal, D., Lunder, C., Mefford, T., Ogren, J. A., Sharma, S., Spichtinger, N., Stebel, K., Stone, R., Strm, J., Trseth, K., Wehrli, C., and Yttri, K. E.: Pan-Arctic enhancements of light absorbing aerosol concentrations due to North American boreal forest fires during summer 2004, Journal of Geophysical Research: Atmospheres, 111, D22 214, doi:10.1029/2006JD007216, http://dx.doi.org/10.1029/2006JD007216, 2006.

Stohl, A., Klimont, Z., Eckhardt, S., Kupiainen, K., Shevchenko, V. P., Kopeikin, V. M., and Novigatsky, A. N.: Black carbon in the Arctic: the underestimated role of gas flaring and residential combustion emissions, Atmospheric Chemistry and Physics, 13, 8833–8855, doi:10.5194/acp-13-8833-2013, http://www.atmos-chem-phys.net/13/8833/2013/, 2013.

Vaughan, M. A., Powell, K. A., Winker, D. M., Hostetler, C. A., Kuehn, R. E., Hunt, W. H., Getzewich, B. J., Young, S. A., Liu, Z., and McGill, M. J.: Fully Automated Detection of Cloud and Aerosol Layers in the CALIPSO Lidar Measurements, J. Atmos. Oceanic Technol., 26, 2034–2050, doi:10.1175/2009JTECHA1228.1, http://dx.doi.org/10.1175/2009JTECHA1228.1, 2009.

Vaughan, M. A., Liu, Z., McGill, M. J., Hu, Y., and Obland, M. D.: On the spectral dependence of

backscatter from cirrus clouds: Assessing CALIOP's 1064 nm calibration assumptions using cloud physics lidar measurements, Journal of Geophysical Research: Atmospheres, 115, D14 206, doi:10.1029/2009JD013086, http://dx.doi.org/10.1029/2009JD013086, 2010.

Vaughan, M. A., Garnier, A., Liu, Z., Josset, D., Hu, Y., Lee, K.-P., Hunt, W., Vernier, J.-P., Rodier, S., Pelon, J., and Winker, D.: Chaos, consternation and CALIPSO calibration: new strategies for calibrating the CALIOP 1064 nm Channel, in: Proceedings of the 26th Int. Laser Radar Conf., Porto Heli, Greece, pp. 39–55, Alexandros Papayannis, University of Athens, Greece, 2012.

Vernier, J.-P., Pommereau, J.-P., Garnier, A., Pelon, J., Larsen, N., Nielsen, J., Christensen, T., Cairo, F., Thomason, L. W., Leblanc, T., and Mcdermid, I. S.: Tropical stratospheric aerosol layer from CALIPSO lidar observations, Journal of Geophysical Research Atmospheres, 114, D00H10, doi:10.1029/2009JD011946, 2009.

Warneke, C., Froyd, K. D., Brioude, J., Bahreini, R., Brock, C. A., Cozic, J., de Gouw, J. A., Fahey, D. W., Ferrare, R., Holloway, J. S., Middlebrook, A. M., Miller, L., Montzka, S., Schwarz, J. P., Sodemann, H., Spackman, J. R., and Stohl, A.: An important contribution to springtime Arctic aerosol from biomass burning in Russia, Geophys. Res. Lett., 37, L01 801, doi:10.1029/2009GL041816, http://dx.doi.org/10.1029/2009GL041816, 2010.

Winker, D. M., Vaughan, M. A., Omar, A., Hu, Y., Powell, K. A., Liu, Z., Hunt, W. H., and Young, S. A.: Overview of the CALIPSO Mission and CALIOP Data Processing Algorithms, J. Atmos. Oceanic Technol., 26, 2310–2323, doi:10.1175/2009JTECHA1281.1, http://dx.doi.org/10.1175/2009JTECHA1281.1, 2009.

Winker, D. M., Tackett, J. L., Getzewich, B. J., Liu, Z., Vaughan, M. A., and Rogers, R. R.: The global 3-D distribution of tropospheric aerosols as characterized by CALIOP, Atmospheric Chemistry and Physics, 13, 3345–3361, doi:10.5194/acp-13-3345-2013, http://www.atmos-chem-phys.net/13/3345/2013/, 2013.

Wu, D. L., Chae, J. H., Lambert, A., and Zhang, F. F.: Characteristics of CALIOP attenuated backscatter noise: implication for cloud/aerosol detection, Atmospheric Chemistry and Physics, 11, 2641–2654, doi:10.5194/acp-11-2641-2011, http://www.atmos-chem-phys.net/11/2641/2011/, 2011.

Yoon, Y. J., Ceburnis, D., Cavalli, F., Jourdan, O., Putaud, J. P., Facchini, M. C., Decesari, S., Fuzzi, S., Sellegri, K., Jennings, S. G., and O'Dowd, C. D.: Seasonal characteristics of the physicochemical properties of North Atlantic marine atmospheric aerosols, Journal of Geophysical Research: Atmospheres, 112, doi:10.1029/2005JD007044, http://dx.doi.org/10.1029/2005JD007044, 2007.

Table 1. Time and positions of the airborne lidar vertical cross sections measured during the POLARCAT campaign

Flight	Date	Start Time	End time	Start latitude	End latitude
24	2008/03/30	13:40 UT	14:15 UT	72.2	71.2
25	2008/03/31	11:30 UT	12:00 UT	71	72.3
26	2008/04/01	10:50 UT	11:15 UT	71.2	72.3
27	2008/04/03	08:15 UT	09:15 UT	68	71
27	2008/04/03	08:50 UT	09:50 UT	71	68
28	2008/04/06	12:30 UT	13:30 UT	69	72.7
29	2008/04/07	08:45 UT	09:15 UT	69.5	71
29	2008/04/07	10:20 UT	11:10 UT	72	70
30	2008/04/07	13:10 UT	13:45 UT	69.8	68
31	2008/04/08	08:45 UT	09:45 UT	68	71
31	2008/04/08	10:45 UT	11:30 UT	72	70
32	2008/04/08	13:10 UT	13:45 UT	70	68
33	2008/04/09	09:10 UT	09:50 UT	68	70.5
33	2008/04/09	11:00 UT	12:10 UT	71.5	67.8
34	2008/04/10	10:20 UT	11:20 UT	68	72
34	2008/04/10	12:45 UT	13:15 UT	70	68
35	2008/04/11	10:00 UT	11:30 UT	72.2	71.2
35	2008/04/11	12:30 UT	12:55 UT	69.2	68.2

Table 2. Comparison of mean aerosol layer pseudo (CR) and aerosol (CRa) color ratio measured by the B-LNG lidar and in-situ measurements: CO mixing ratio, Grimm integral and CPC concentrations, and the mean aerosol diameter from the SMPS+GRIMM spectrum. Layers with green or yellow color are respectively for low or high value of CR.

Date Time (UT)	lat.,dg	alt. km	CO ppbv	CR B-LNG	CRa B-LNG	CPC cm^{-3}	Grimm cm^{-3}	Dmean μm
30/03/08 13:45	72.0N	2.2	166	17.5±1.5%	38±6%	500	300	0.22
07/04/08 09:05	70.3N	4.5	153	8.7±2%	39±64%	450	50	0.07
08/04/08 11:20	70.7N	5.0	140	14.5±2.3%	62±44%	330	25	0.13
08/04/08 13:12	69.9N	1.0	153	10.0±1.5%	19±6%	800	25	0.07
08/04/08 13:17	69.7N	4.5	200	14.7±1.6%	27±6%	800	70	0.16
08/04/08 13:50	68.4N	4.0	220	17.0±1.5%	28±4%	1000	150	0.18
09/04/08 11:30	69.9N	4.5	210	10.0±1.8%	26±16%	2500	74	0.07
07/04/08 10:15	69.0N	4.0	210	11.0±1.4%	19±5%	1000	50	0.12
07/04/08 10:35	69.6N	3.5	230	18.7±1.5%	31±4%	900	300	0.22
07/04/08 11:05	71.6N	3.5	200	17.0±1.6%	42±6%	700	250	0.18

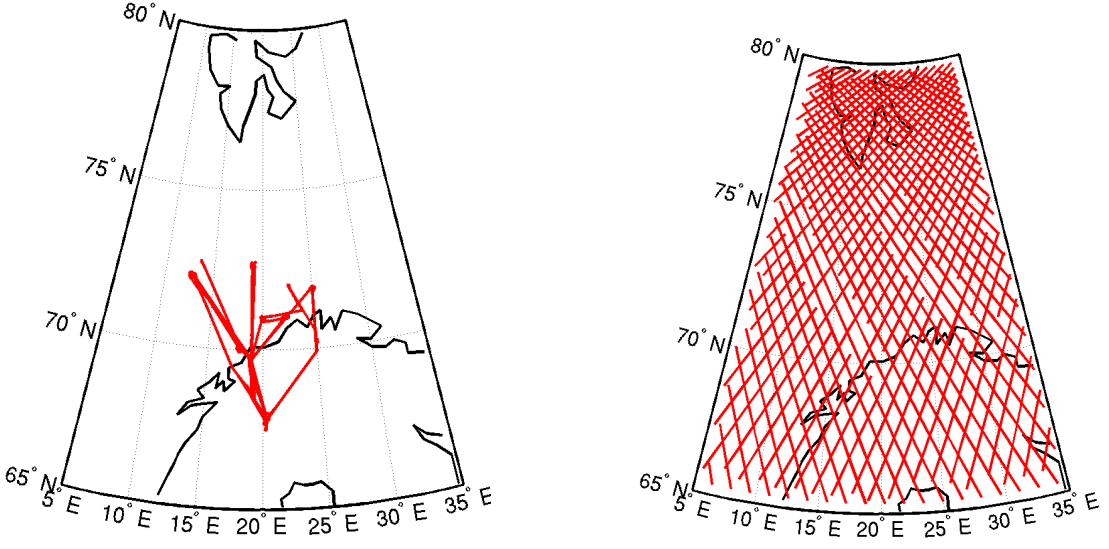

Fig. 1. Aircraft trajectories for the measurement days listed in Table 1 (left) and positions of the CALIOP tracks from 27 March to 11 April (right).

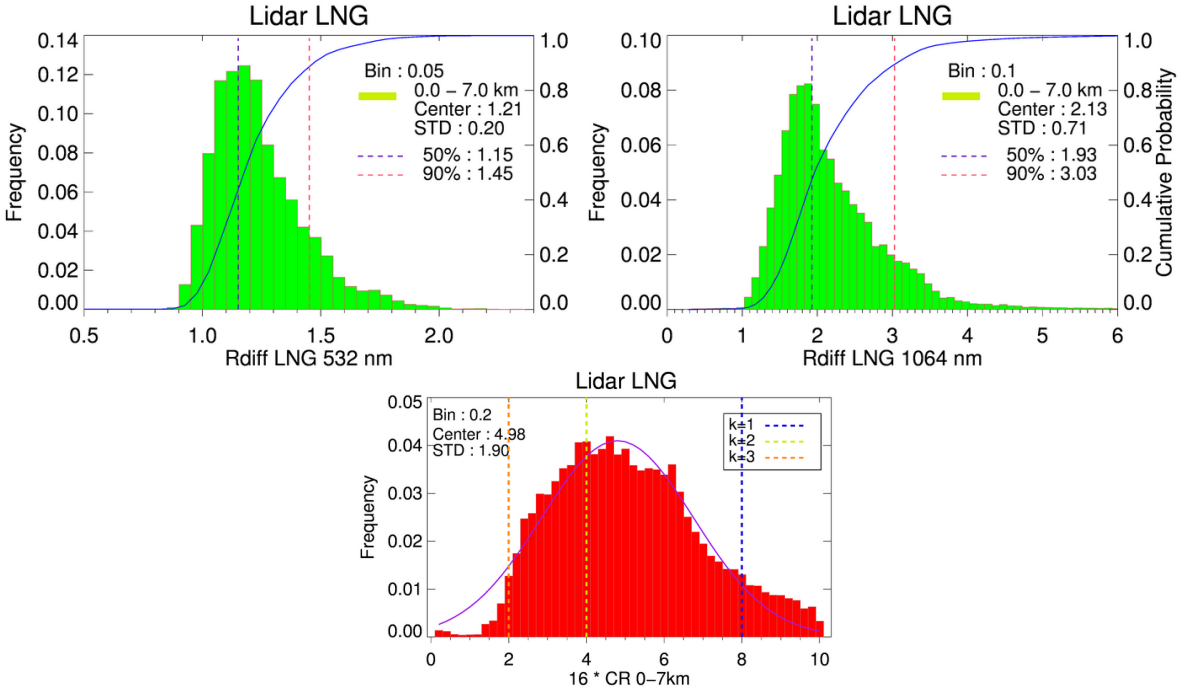

Fig. 2. Distribution and cumulative probability (blue) of the 532 nm (left), 1064 nm (middle) backscatter ratios measured by the airborne lidar from 30 March 30 to 11 April. Mean, standard deviation, median and 90th percentile are given for each distribution. The distribution of the aerosol color ratio CR_a*16 (right panel) is compared to the lines for CR_a=0.125 (k=3), CR_a=0.25 (k=2) or CR_a=0.5 (k=1)

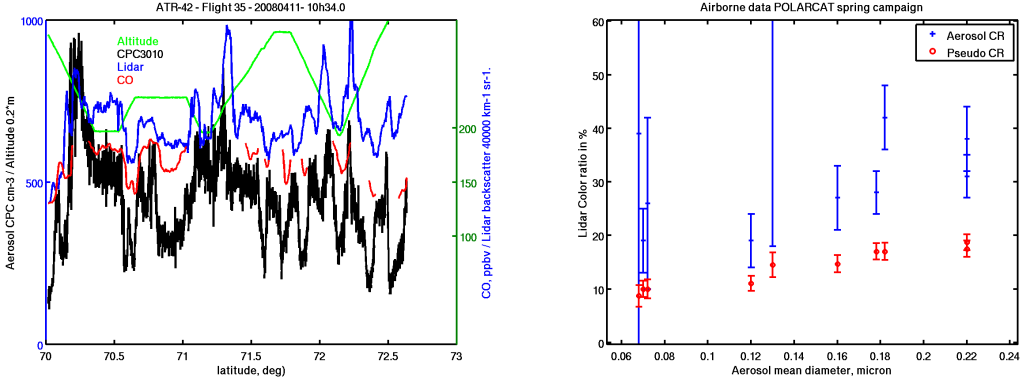

Fig. 3. (left) Comparison of lidar attenuated backscatter 120 m to 200 m below the aircraft in relative units with in-situ measurements of CO (red) in ppbv, and aerosol concentration (black) in particles per cm^{-3} for a flight (35) with crossing of several aerosol layers. Green curve is the aircraft altitude in 5 m unit. (right) Lidar color ratios (pseudo CR for total backscatter and aerosol CR for aerosol backscatter) in % for 10 aerosol layers where in-situ and lidar data can be compared (see table 2) versus the SMPS aerosol mean diameter.

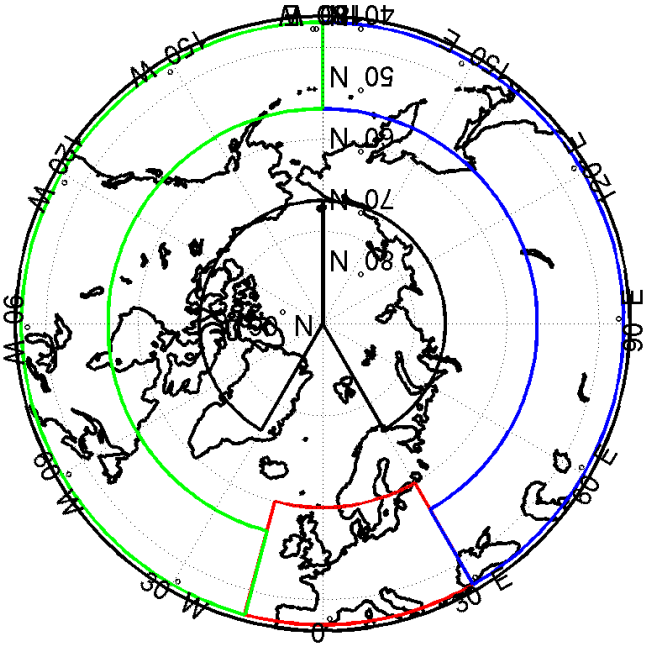

Fig. 4. Map of the regions selected to study the origin of the air masses in the FLEXPART analysis. The red, green and blue boxes correspond to our definition of the European, North American and Eurasian regions. The two black boxes are called western and eastern Arctic regions.

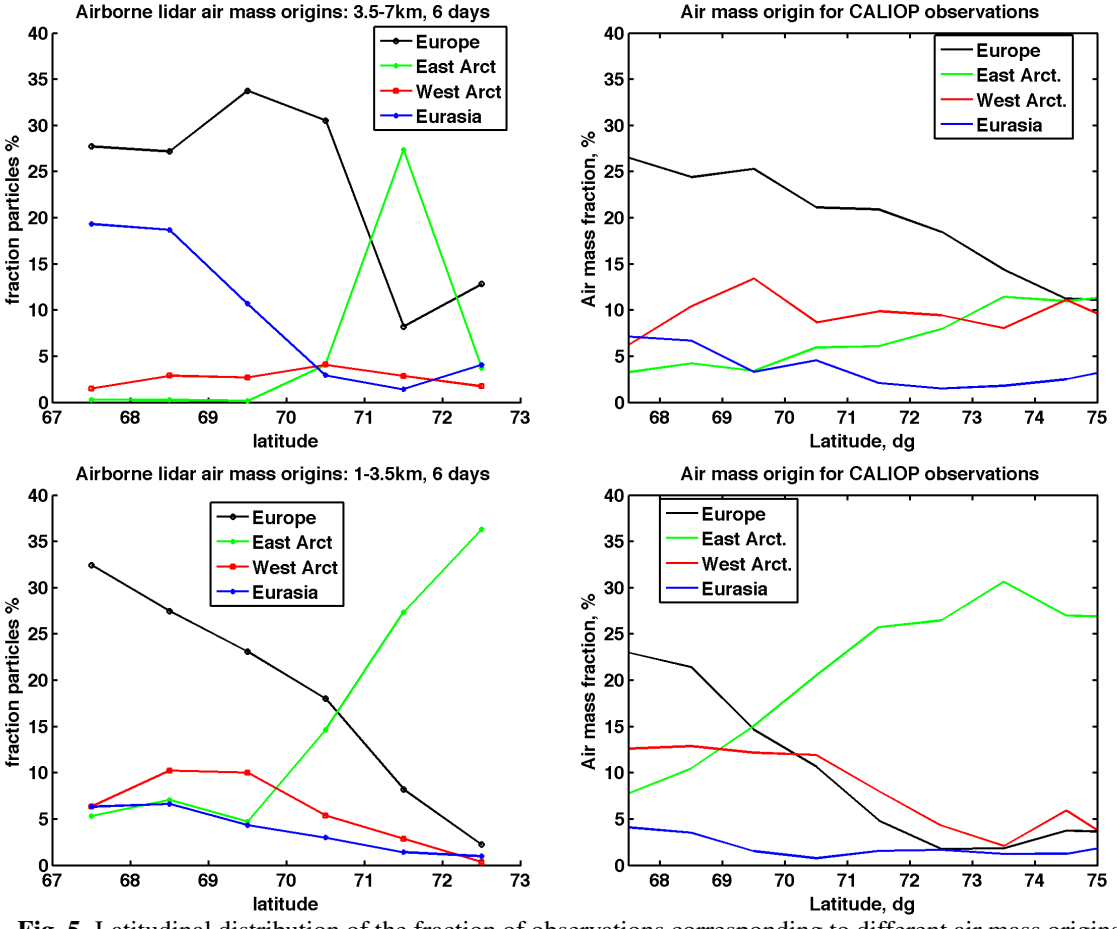

Fig. 5. Latitudinal distribution of the fraction of observations corresponding to different air mass origins calculated with FLEXPART for the airborne lidar (left column) and CALIOP observations (right column) at altitudes < 3 km (bottom row) and between 3 and 7 km (top row).

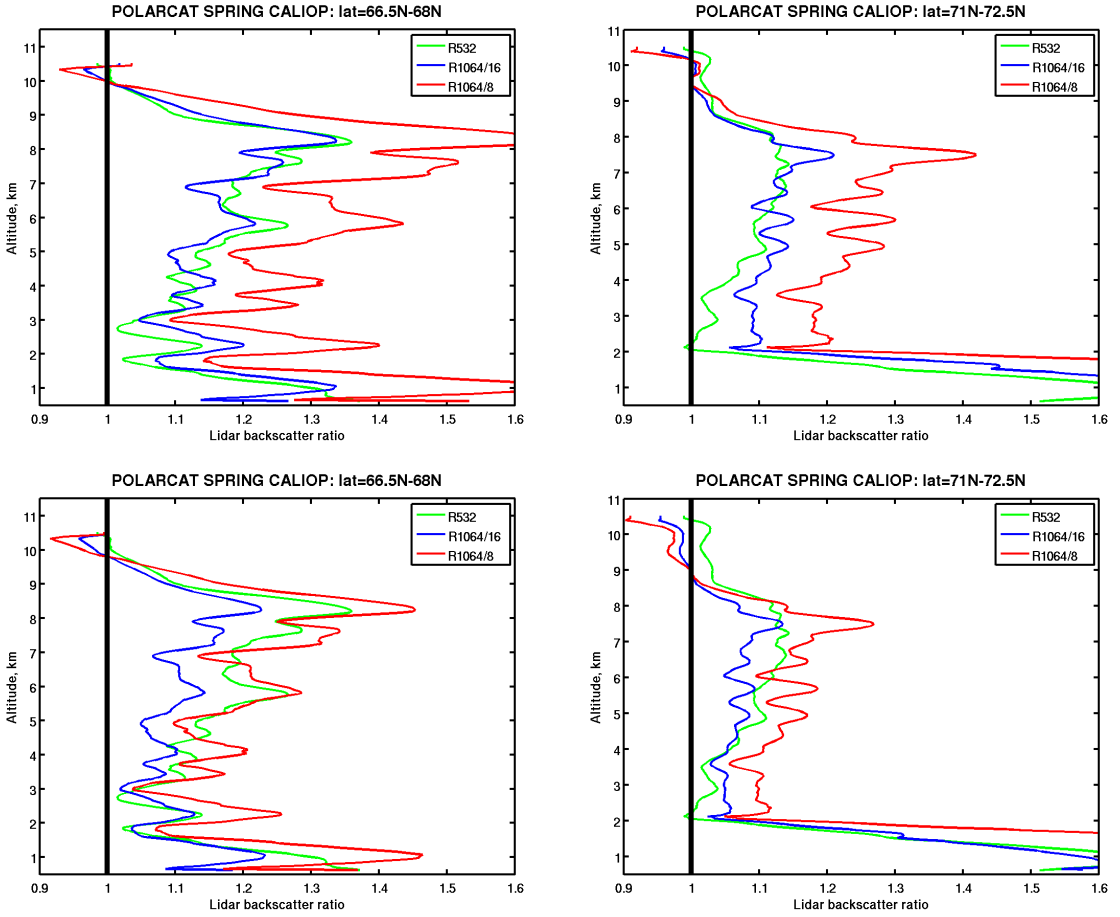

Fig. 6. Mean attenuated backscatter ratio for the 532 nm (green) and 1064 nm filtered level 1 CALIOP (blue and red). The 1064 nm values are scaled to the 532 nm values using expected largest CR_a=0.5 (red) and lowest CR_a=1 (blue). The top and bottom row are for respectively ~~calibration~~ uncorrected and calibration corrected IR data.

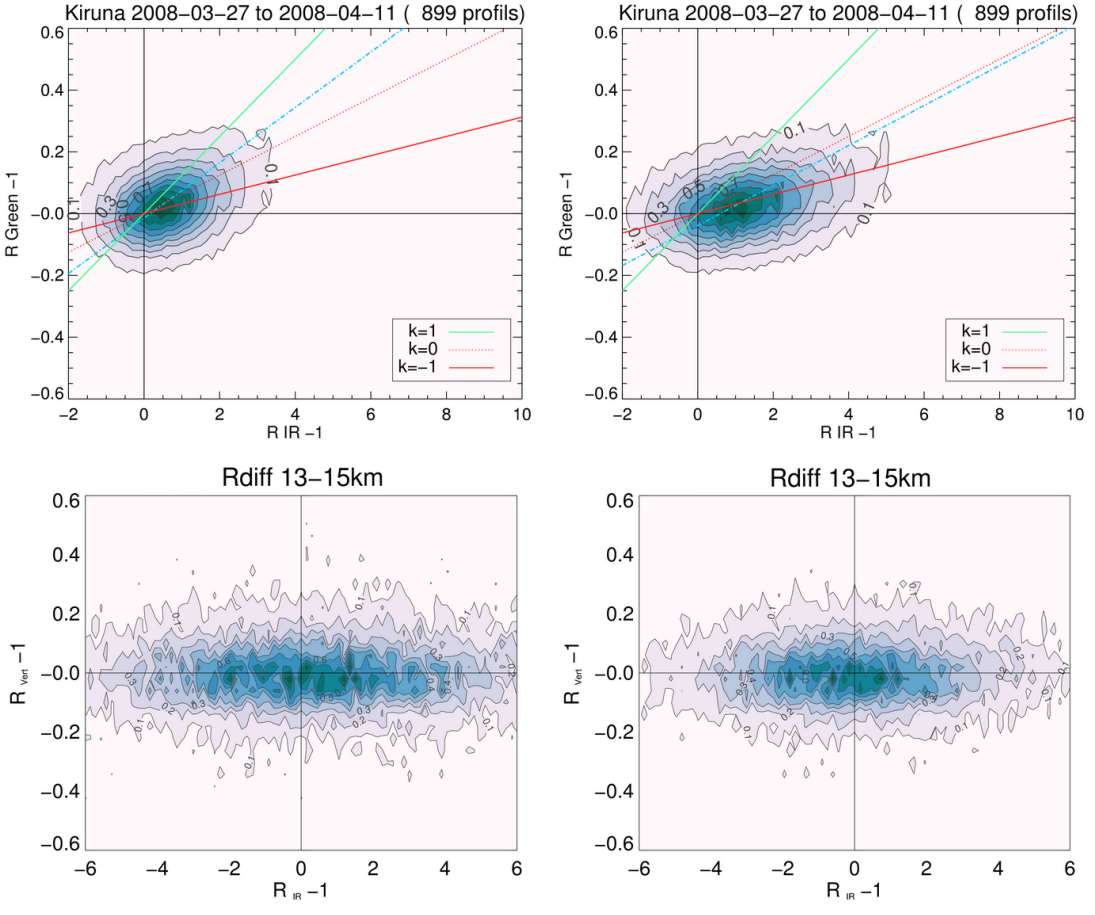

Fig. 7. Correlation between the 532 nm and 1064 nm mean backscatter ratio measured by filtered level 1 CALIOP from 27 March to 11 April 2008, at altitudes from 0 to 7 km (top row) and 13 to 15 km (bottom row) using either uncorrected (left) or corrected (right) IR backscatter data. Regression line is the dashed-dotted blue line. The lines k=-1, 0, 1 are respectively for tropospheric aerosol distribution with CR_a=2, 1, 0.5.

.

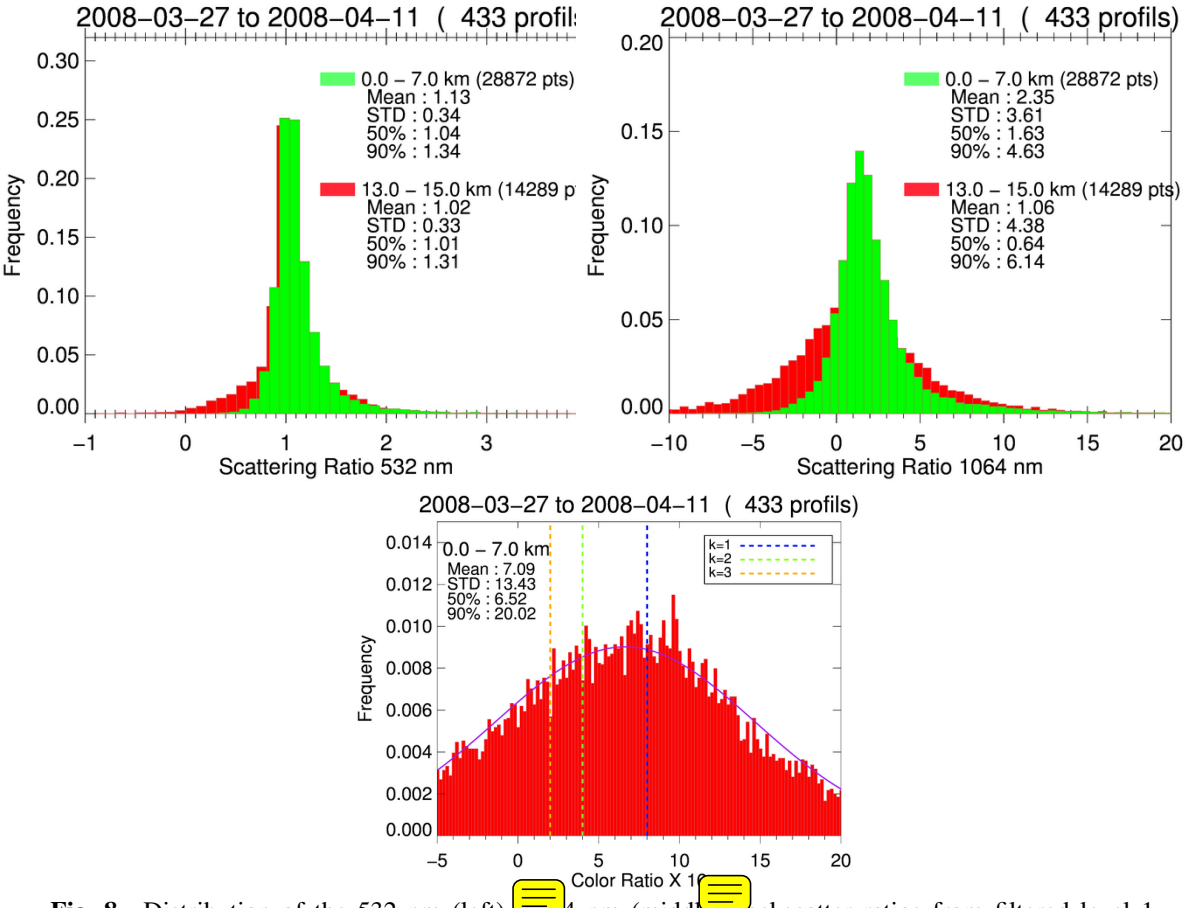

Fig. 8. Distribution of the 532 nm (left), 1064 nm (~~middle~~) backscatter ratios from filtered level 1 CALIOP data at altitudes from 0 to 7 km (green) and 13 to 15 km (red) from 27 March to 11 April in the aircraft flight area. Mean, standard deviation, median and 90th perc[illegible]e are given for each distribution. The maximum of the aerosol color ratio $16*CR_a$ distribution (right panel) is compared to the lines for CR_a=0.125 (k=3), CR_a=0.25 (k=2) or CR_a=0.5 (k=1)

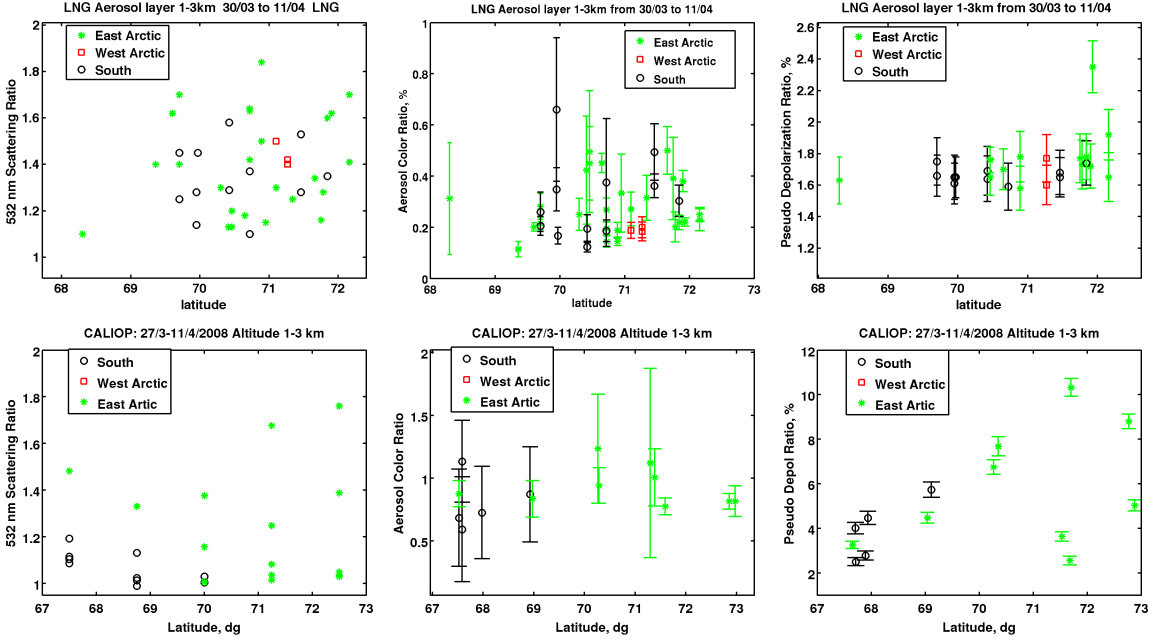

Fig. 9. Latitudinal distribution of 532 nm backscatter ratio (left), aerosol color ratio (middle) and pseudo depolarization ratio (right) for the airborne lidar observations (top) and filtered level 1 CALIOP (bottom) at altitudes < 3 km during the aircraft campaign. The colors are for different air mass origins estimated with Flexpart (see text).

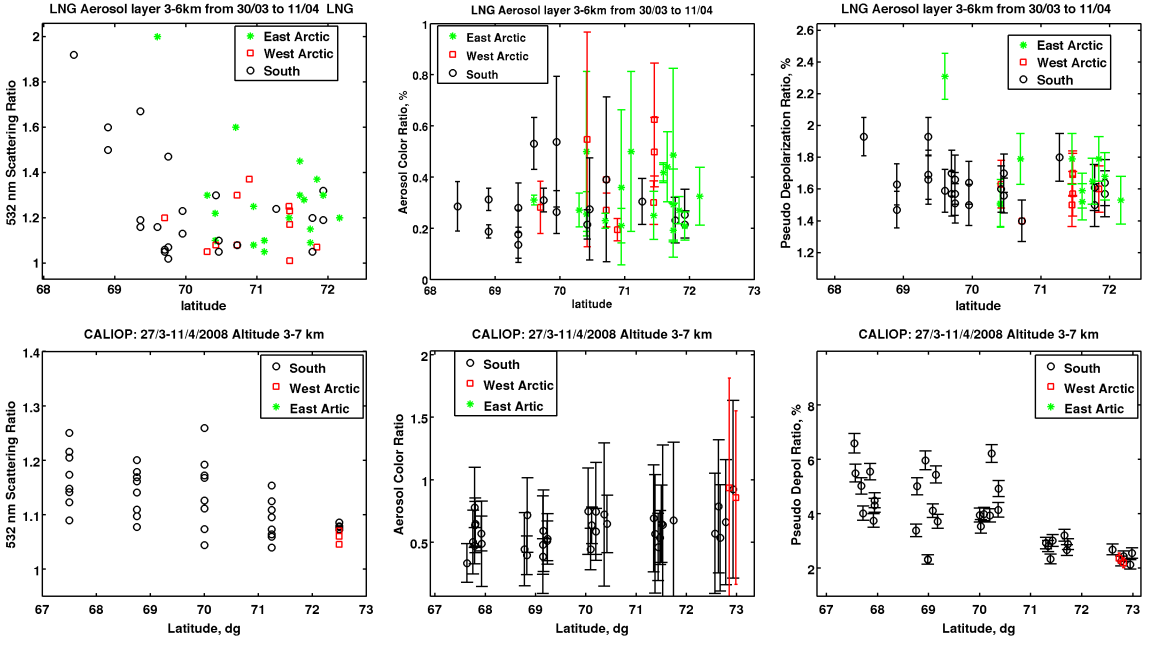

Fig. 10. Latitudinal distribution of 532 nm backscatter ratio (left), aerosol color ratio (middle) and pseudo depolarization ratio (right) for the airborne lidar observations (top) and filtered level 1 CALIOP (bottom) at altitudes between 3 km and 7 km during the aircraft campaign. The colors are for different air mass origins estimated with Flexpart (see text).

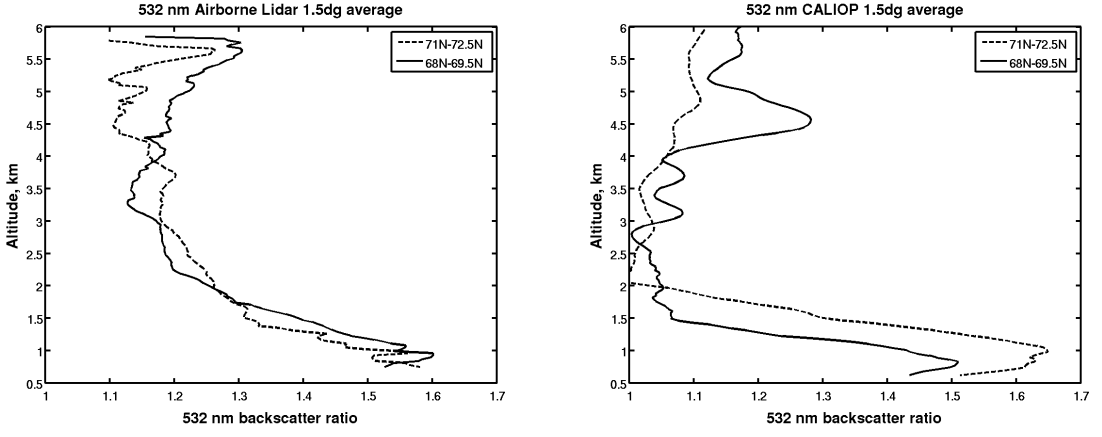

Fig. 11. Mean 532-nm backscatter ratio vertical profile over a 1.5 °latitude band for the airborne lidar data (left) and filtered level 1 CALIOP data (right)

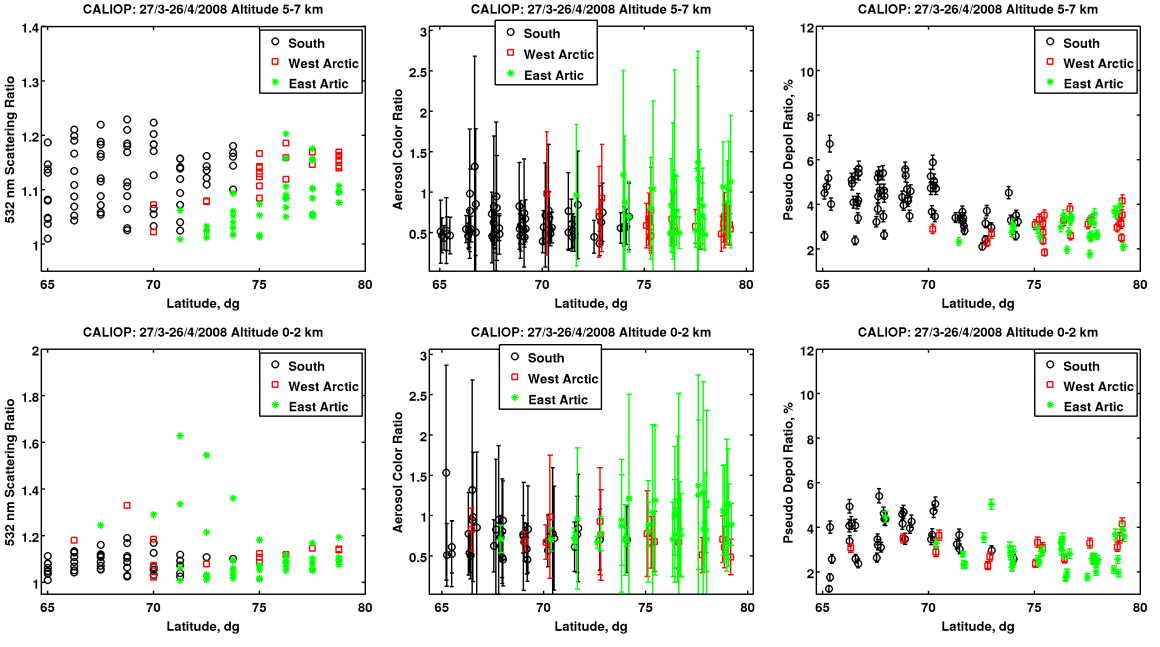

Fig. 12. Latitudinal distribution of 532 nm backscatter ratio (left), aerosol color ratio (middle) and pseudo depolarization ratio (right) for filtered level 1 CALIOP in April 2008 at altitudes < 2 km (bottom) and between 5 km and 7 km (top). The origin of the layers are estimated with Flexpart (see text).

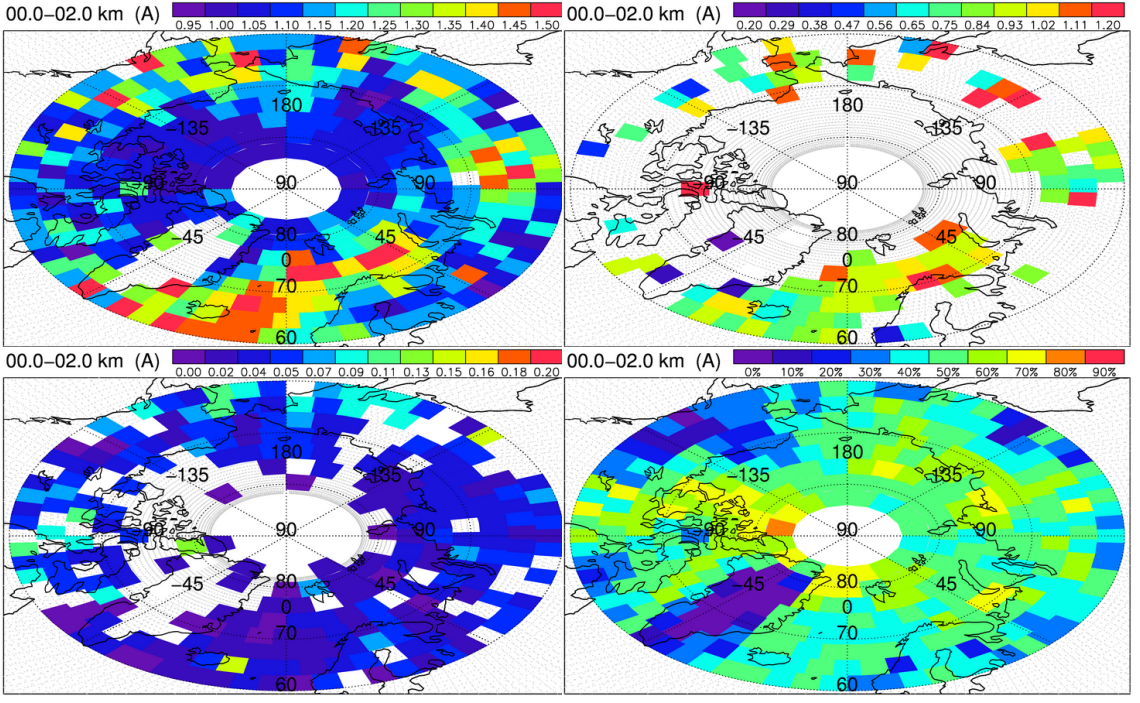

Fig. 13. Map of the 532 nm backscatter ratio, aerosol color ratio, pseudo depolarization ratio and fraction of cloudless observations using the April 2008 filtered level 1 CALIOP data in the 0-2 km altitude range.

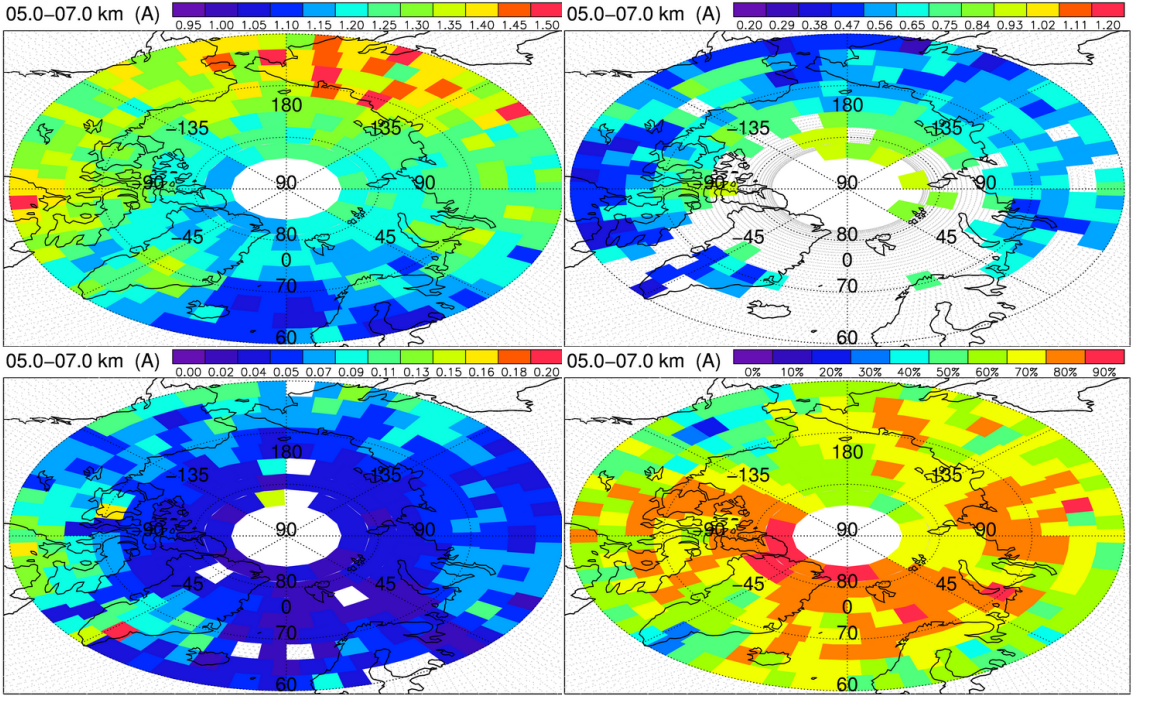

Fig. 14. Map of the 532 nm backscatter ratio, aerosol color ratio, pseudo depolarization ratio and fraction of cloudless observations using the April 2008 filtered level 1 CALIOP data in the 5-7 km altitude range.

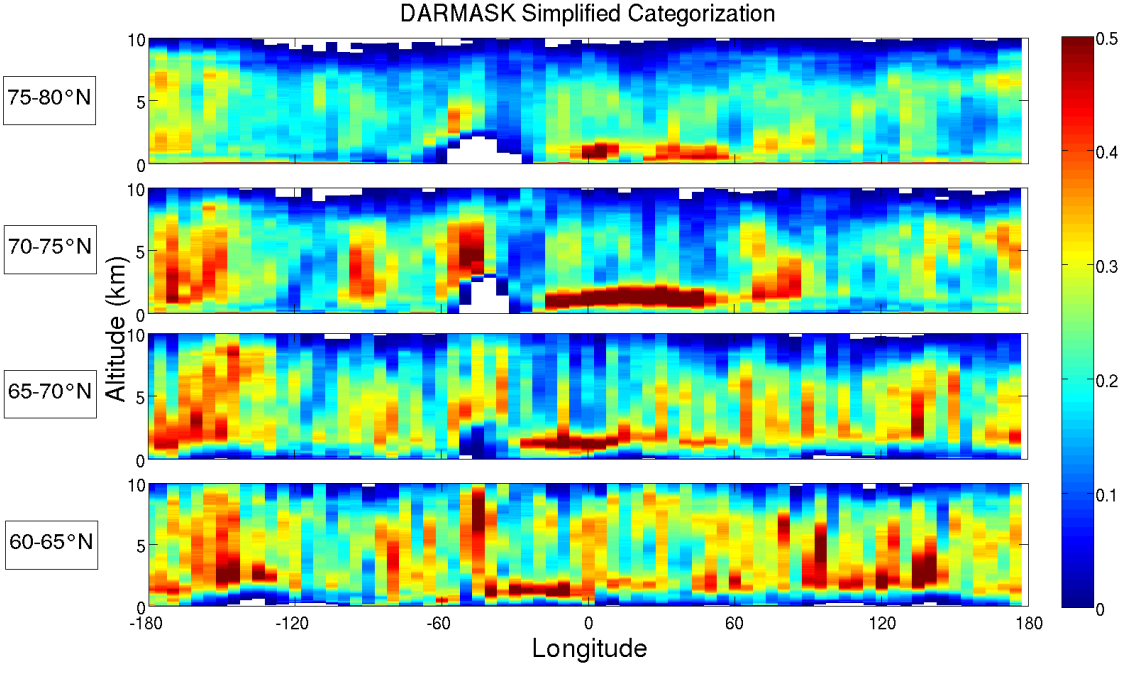

Fig. 15. Zonal vertical cross sections of the cloud fraction derived from the DARDAR products for April 2008 in 4 latitude bands from 60°N to 80°N. The longitudinal resolution is 5°and the vertical resolution is 60 m.